DLR-IB-RM-OP-2019-30

Natural Gait Discovery for Compliantly Actuated Legged Robots

Master's Thesis

Anna Sesselmann

DLR Deutsches Zentrum für Luft- und Raumfahrt

DEPARTMENT OF INFORMATICS

TECHNICAL UNIVERSITY OF MUNICH

Master's Thesis in Robotics, Cognition, Intelligence

Natural Gait Discovery for Compliantly Actuated Legged Robots

Anna Sesselmann

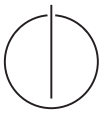

DEPARTMENT OF INFORMATICS

TECHNICAL UNIVERSITY OF MUNICH

Master's Thesis in Robotics, Cognition, Intelligence

Natural Gait Discovery for Compliantly Actuated Legged Robots

Entdeckung natürlicher Gangarten für elastisch angetriebene Laufroboter

Author: Anna Sesselmann
Supervisor: Prof. Dr. Alin Albu-Schäffer
Advisor: Dr. Dominic Lakatos
Date: January 15th, 2019

I confirm that this master's thesis is my own work and I have documented all sources and material used.

Garching, January 15th, 2019 Anna Sesselmann

Abstract

Nature evolved legs to travel in difficult terrain. Biological legged locomotion displays different gaits to minimize the energy needed to move with certain velocities. For example, humans walk with low velocity but switch to running when moving faster. Robotic legged locomotion proves to be a challenging topic. Most state-of-the-art motion planning approaches heavily control legged robotic systems in order to perform aspired movements. Changing the intrinsic dynamics of the system through control is necessary since the dynamics do not inherently exhibit the desired motions. However, recent work suggests that embedding desired dynamics into segmented robotic legs reduces the necessity of extensive control.

This Master's Thesis combines theoretical templates for legged locomotion with physically realizable robotic legs. It first presents energy-conservative spring-loaded inverted pendulum (SLIP) models, which explain the existence of different gaits in legged locomotion. These templates are modified to capture the effects of physical damping and ground contact dynamics. A minimal control action compensates the resulting energy losses. Hereby, several natural gaits could be displayed with a non-conservative SLIP model. Based on this newly developed model, a segmented leg featuring a pantograph mechanism is designed. The inherent dynamics of this robotic leg are matched with the SLIP dynamics of the non-conservative template model. Based on optimized design parameters, the influence of deviating parameters on the natural dynamics is analyzed. These imprecisions occur when physically realizing the robotic leg.

Natural gaits can be transferred from energy-conservative SLIP models to non-conservative models. SLIP-like dynamics are embedded into segmented legs, which can reduce the control necessary to exhibit periodic motions. Gaits supported by the intrinsic dynamics result in reduced energy consumption.

Contents

Abstract **iii**

List of Abbreviations **vi**

1 Introduction **1**
1.1 Motivation 1
1.2 Related Work 1
1.3 Goal of the Thesis 2
1.4 Structure 2

2 Foundation **4**
2.1 Spring Loaded Inverted Pendulum (SLIP) Model 4
2.2 Extended SLIP Model 5
2.3 Gait Definition 7
2.4 Mathematical Tools 7
2.4.1 Poincaré Section 7
2.4.2 Continuation 8
2.4.3 Floquet Analysis 8
2.4.4 Bifurcations 9

3 Non-Conservative SLIP Model **10**
3.1 Dynamic Model 10
3.2 Hybrid Dynamics 11
3.2.1 Continuous Dynamics 11
3.2.2 Discrete Dynamics 13
3.2.3 Energy Fluctuation 14
3.3 Search for Periodic Motions 15
3.3.1 Periodic Motion 16
3.3.2 Event Detection 16
3.3.3 Timing Variables 17
3.3.4 Comparison of Event Detection and Timing Variables 18
3.3.5 Multi-Legged Systems 19
3.4 Bipedal Model 20

3.5 Gaits . . . 21
3.5.1 Method . . . 21
3.5.2 One-Leg Hopper . . . 23
3.5.3 Biped . . . 26

4 Pantograph Leg **30**
4.1 Dynamic Model . . . 30
4.2 Hybrid Dynamics . . . 31
4.3 Modal Dynamics Matching . . . 32
4.3.1 Task Coordinates . . . 33
4.4 Search for Optimal Design Parameters . . . 34
4.4.1 Design Parameters . . . 35
4.4.2 Eigenfrequency Matching . . . 36
4.5 Analysis of the Results . . . 38
4.6 Comparison to Biological Legs . . . 41

5 Discussion **42**
5.1 Non-Conservative SLIP Model with Minimal Control . . . 42
5.2 Natural Gaits of the Non-Conservative SLIP Models . . . 43
5.3 Eigenfrequency Matching of the Pantograph Leg . . . 44

6 Conclusion **45**
6.1 Future Work . . . 46
6.1.1 Non-Conservative SLIP Model . . . 46
6.1.2 Pantograph Leg . . . 46

List of Figures **47**

List of Tables **48**

Bibliography **49**

List of Abbreviations

CoM	Center of Mass
DoF	Degree of Freedom
GRF	Ground Reaction Force
IP	Inverted Pendulum
SLIP	Spring-Loaded Inverted Pendulum

Chapter 1

Introduction

This thesis is written with the Chair of Sensor Based Robotic Systems and Intelligent Assistance Systems at TUM, in cooperation with the Institute of Robotics and Mechatronics at the German Aerospace Center (DLR). It addresses the question of how natural gaits of legged biological systems transfer to legged robotic systems.

1.1 Motivation

Nature has found the best way to move in difficult terrain. Legged locomotion minimizes energy consumption per velocity. Bipedal locomotion uses a walking gait for low velocities and switches to a running gait for high velocities. Quadrupedal mammals walk when traveling at low velocity. With increasing velocity, the gait switches to trotting and for high velocities to galloping. Since gaits have an optimal velocity range in which they are most efficient, switching between gaits allows the biological system to move with minimal energy. We want to transfer the characteristics of natural gaits to legged robots to reduce the energy consumption of locomotion.

Walking, trotting, and galloping are found across many species of quadrupedal mammals. This leads to the hypothesis that gaits are not a mean of control, but rather embedded in the dynamics of the mammalian body. Different gaits can be regarded as oscillations of one system on different energy levels. We want to integrate these dynamics into robotic legs to reduce the amount of control and energy necessary to exhibit legged locomotion.

1.2 Related Work

There are several approaches to reduce the complexity of natural legged locomotion. Biological legs store energy in tendons and muscles, which leads to the mechanical representation of the leg as a spring. Blickhan [1989] proposed a simple spring-mass model as a template for a natural leg. This

model exhibits ground reaction forces while hopping which closely resemble those occurring in running biological systems. This model is referred to as the spring-loaded inverted pendulum (SLIP) model. Geyer et al. [2006] added a second leg spring to the spring-mass model. They showed that the bipedal SLIP model not only displays running gaits but also walking gaits. The key aspect of producing the ground reaction force profile of natural walking was proven to be the double support phase. A drawback of these models is, that only the dynamics of the stance phase are modeled. The leg angle in flight phase is static, resulting in the absence of swing leg dynamics. Gan et al. [2018b] extended the bipedal SLIP model to incorporate a swing leg dynamic. This led to the discovery of a wide variety of bipedal gaits never before shown in reduced template models. Most SLIP-based models of legged locomotion reported in literature so far are energy-conservative, taking the impact of contact dynamics not into account.

Movement in complex terrains requires segmented legs. Periodic motions of a leg can be described with the length and the angle of the leg. Hereby, the leg length is the distance between the hip and foot, and the connecting line between hip and foot defines the leg angle. Lakatos et al. [2017] proposed a matching procedure to embed desired oscillation modes present in legged locomotion into the dynamics of an articulated robotic leg. The locomotion of this leg is defined by its natural dynamics, which results in energy-efficient movements. The intrinsic dynamics of the leg do not need to be changed by control, rather control excites the natural dynamics to replace energy lost through friction and ground contact. The study proposes a pantograph leg mechanism as an ideal robotic system to integrate SLIP-like dynamics. This segmented leg features a pantograph mechanism and closely resembles mammalian legs.

1.3 Goal of the Thesis

This thesis aims at transferring natural gaits to legged robots on the basis of the introduced concepts. First, a non-conservative SLIP model is built. It is used to study whether energy fluctuations in a periodic motion influence the existence of natural gaits. Secondly, the natural gaits found in conservative models are transferred to our new model. Thirdly, a pantograph leg is parametrized to display SLIP-like dynamics and a natural gait is demonstrated.

1.4 Structure

The structure of this thesis closely follows the chronological order in which the research was conducted.

Chapter 2 talks about the foundation needed to understand the reasoning and methods used in the following chapters. The bipedal SLIP model, as well as its extensions, are thoroughly explained. The definition and characterization of a gait and stride are presented. In the end, the theory behind the generation, analysis, and evaluation of our results are introduced.

Chapter 3 extensively explains our modifications in the dynamics of the extended SLIP model and how the hybrid dynamics is computed. Furthermore, it explains the details of our search for different gaits and in the end presents and evaluates all gaits found.

Chapter 4 introduces the pantograph leg with SLIP-like dynamics. It explains the restrictions on and the process of choosing the physical parameters. Furthermore, the so-parametrized leg is compared to biological legs.

Chapter 5 discusses the relevance of this work. In chapter 6, all findings are summarized, and future work on the non-conservative SLIP model and the pantograph leg model is presented.

Chapter 2

Foundation

This chapter introduces the history of templates for legged locomotion. Furthermore, the terms *gait* and *stride* are defined. In the end, the mathematical theory of gait analysis is explained.

2.1 Spring Loaded Inverted Pendulum (SLIP) Model

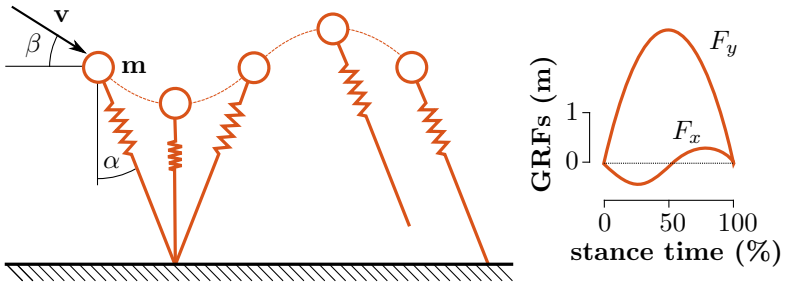

Figure 2.1: One stride of a running spring-mass system *(Adapted from Blickhan [1989], Fig. 5)*

The SLIP model was first introduced by Blickhan [1989] as "The spring-mass model for running and hopping". It consists of a body point mass m with a massless translational spring with resting length l and stiffness k. This planar model is conservative, has no controller and therefore its motion is only defined by its inherent dynamics. Steady state running can be described by magnitude $\mathbf{v}$, angle β of body velocity at touchdown, and the angle of attack α. The angle of attack complies with the hip angle of a human runner, and describes the direction of the leg when ground contact is established. At touchdown, the leg spring is uncompressed. In stance, the spring compresses and lengthens again, switching to the flight phase when it is fully uncompressed again. After ground contact is broken, the spring

instantly goes in the configuration defined by the angle of attack. Figure 2.1 represents a stride of the system. The plot on the right shows idealized ground reaction forces present during stance. The spring-mass model exhibits hopping and running gaits. The energy conversion of potential and kinetic energy of the CoM is sufficiently similar to the exchange of energies observed in experiments of human running.

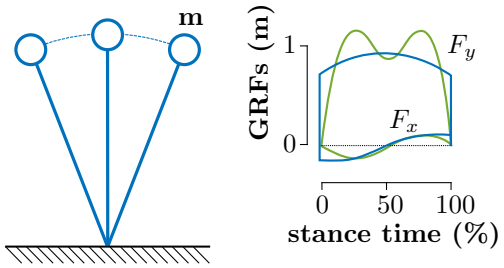

Figure 2.2: Ground reaction forces of the IP model *(Adapted from Geyer et al. [2006])*

Mochon and McMahon [1980] showed that the body CoM position in bipedal walking can be modeled with the inverted pendulum (IP) model. This vaulting over stiff legs nevertheless cannot reproduce the characteristic M-shaped vertical GRF profile of the human walking gait in stance (Figure 2.2). The blue line displays the GRF profile of the IP model in stance, and the green line represents the idealized profile of a human bipedal walker.

Geyer et al. [2006] introduced the bipedal SLIP model. It was created by adding second massless spring with the same stiffness k and resting length l to the spring-mass model. Additionally to running gaits, they found walking gaits replicating the out-of-phase changes of potential and forward kinetic energy, as well as the CoM trajectory observed in human walking. Moreover, they found that the key element of the walking motion is the double support, leading to the characteristic M-shaped GRF profile (Figure 2.3). Their work gave an insight into how a bipedal model with only one set of kinematic parameter values can exhibit walking and running. This endorses the hypothesis that oscillations of this system at different energy levels result in distinctive gaits.

2.2 Extended SLIP Model

The bipedal SLIP model captures stance dynamics. However, the swing leg dynamics is suppressed by the predefined angle of attack. As a result, the swing phase is not defined by a passive dynamic motion. The drawbacks include possible infinitesimal small non-physical swing times, the necessity

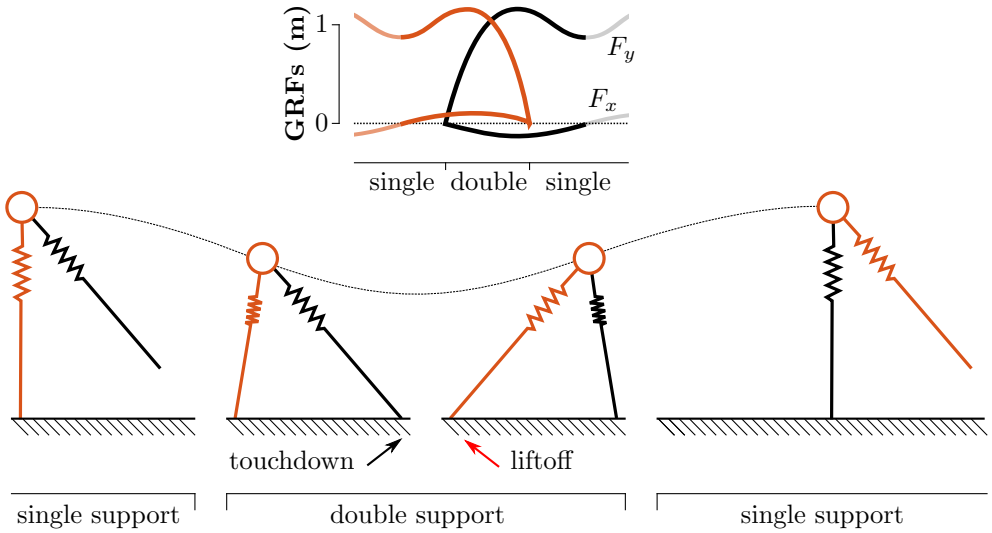

Figure 2.3: One stride of a walking bipedal SLIP model *(Adapted from Geyer et al. [2006])*

to actively adapt the angle of attack to different gaits, and the restriction to gaits with the same angle of attack for both legs.

Gan et al. [2018b] extended the bipedal SLIP model with a torsional spring at the hip joint for both legs. Therefore, the natural mechanical dynamics condition the leg swing. For this polar spring, a swing frequency is defined, rather than a spring stiffness. The latter would demand a foot mass, which would violate the requirement of energy conservation. The angle of the leg and its velocity are now fully defined by the dynamics of the system. The leg length is held constant during swing to prevent infinite small oscillations. The configuration of the system is fully described through its body CoM position and the leg angle α, as well as the corresponding velocities.

The different gaits shown by this model and their connections were extensively analyzed. A variety of gaits was found - including walking, running, skipping, and bipedal galloping - of which some have never been discovered in SLIP models before. A discussion of their results can be found in Section 3.5, together with our own gait analysis.

In addition, the team presented a dynamically complete quadrupedal SLIP model in Gan et al. [2018a]. Their investigations demonstrated how quadrupedal bounding gaits of a model without body pitch are related to bipedal gaits. The hind and front legs of a bounding quadruped move in pairs, making it possible to compare their motions to individual legs of a biped.

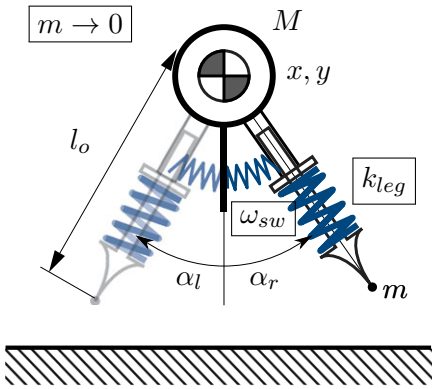

Figure 2.4: Extended SLIP model *(Adapted from Gan et al. [2018b])*

2.3 Gait Definition

A gait is defined as a periodic motion characterized by its initial parameter set X. All states except the horizontal position x of the body return to their initial values after one full stride, causing these gaits to also be called period-1-gaits. We define the beginning and end of a stride without loss of generality to be in the apex. The apex corresponds to zero velocity and a maximum vertical height of the body.

Gait families, e.g. walking or running, are distinguished by their footfall patterns, number of swing leg oscillations and whether the swing leg retracts or not before hitting the ground. The same characteristics are shared by all solutions of one family, for example walking at different speeds always includes a double support phase.

2.4 Mathematical Tools

This section introduces the mathematical theory behind our gait analysis.

2.4.1 Poincaré Section

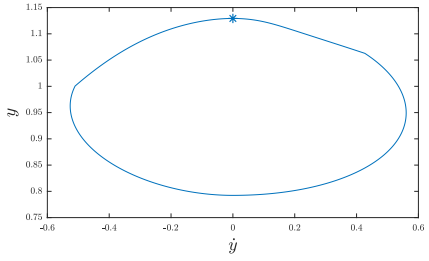

Figure 2.5: Periodic orbit in the y, $\dot{y}$ plane with marked Poincaré section

Figure 2.5 plots the periodic system states of one stride in the y, $\dot{y}$ plane. The marked apex event gives us the Poincaré section used for the analysis of the periodic orbit. The Poincaré map P maps initial states X^o to final states X^{final} after one stride. The state trajectories are obtained through numerical integration of the dynamics of a full stride. Periodicity can be enforced using a zero function (2.1).

$$\Phi := P(X^*) - X^* = \mathbf{0} \tag{2.1}$$

2.4.2 Continuation

Periodic solutions in the Poincaré section evolve along one-dimensional manifolds called 'branches'. Discovering a branch of solutions (e.g. hopping on spot with increasing height) is called continuation (Dankowicz and Schilder [2013]).

Starting with a known solution X_n^* we can find a solution X_{n+1}^* with distance d numerically. The following needs to hold:

- X_{n+1}^* is a periodic solution (2.2)
- it has a fixed distance to the last solution (2.3)
- and the step direction conforms with the last steps direction (2.4)

$$\Phi(X_{n+1}^*) = 0 \tag{2.2}$$
$$||X_{n+1}^* - X_n^*|| = d \tag{2.3}$$
$$(X_{n+1}^* - X_n^*) \cdot (X_n^* - X_{n-1}^*) > 0 \tag{2.4}$$

Finding X_{n+1}^* solving these equations is numerically sensitive to well-guessed initial states X_{n+1}^o. We can generate X_{n+1}^o by either assuming a constant development of solutions (2.5) or by utilizing the results of the Floquet analysis of the Poincaré map.

$$X_{n+1}^o = X_n^* + d \cdot (X_n^* - X_{n-1}^*) \tag{2.5}$$

Continuation is in fact a Prediction-Correction-Process, with (2.5) or the Floquet Analysis (see Section 2.4.3) proposing methods on predicting nearby solutions X_{n+1}^o, and (2.2)-(2.4) giving the conditions for correcting the guess.

2.4.3 Floquet Analysis

Disturbing a stable X_n^* in any direction not along the branch by a small Δx results in a return of the system to X_n^*. A disturbance in the direction of

X^*_{n+1}, however, will result in the system staying on the new trajectory. This characteristic is exploited by the Monodromy matrix $J_n = \frac{\partial P}{\partial X}\big|_{X^*_n}$.

It evaluates the partial derivative of the Poincaré map P with respect to the system states at a periodic solution X^*_n. It approximates the effects of a small change of system states on the system states after one stride. We approximate the Monodromy matrix numerically by computing the central differential quotients for all states of $X^*_{n,i}$. $X^+_{n,i}$ and $X^-_{n,i}$ denote periodic solutions $X^*_{n,i}$, where the ith component has been disturbed by a small Δx in positive (respective negative) direction (2.6).

$$J_{n,i} = \frac{P(X^+_{n,i}) - P(X^-_{n,i})}{2 \cdot \Delta x} \tag{2.6}$$

The eigenvalues $\lambda_{n,i}$ of J_n are called Floquet Multipliers, and for X^*_n being a solution to a periodic system there must be one with value $+1$. The corresponding eigenvector $v_{n,i}$ is tangential to the solution branch and therefore points towards X^*_{n+1}. With $v_{n,i}$ having unit length, the guess for the next solution is computed by (2.7).

$$X^o_{n+1} = X^*_n + d \cdot v_{n,i} \tag{2.7}$$

The step size d can be chosen arbitrarily. Larger values lead to a faster discovery of the solution branch, but might compute initial guesses that do not converge to a periodic solution. Smaller step sizes significantly increase to computation time of discovering a whole solution branch, but produce closer guesses of neighboring solutions.

2.4.4 Bifurcations

Different gait solution branches connect at bifurcation points. Bifurcations occur when there is more than one Floquet multiplier with a value $+1$. A bifurcation marks a break in the symmetry of the solution. The additional eigenvectors $v_{n,i}$ are not tangential to the former solution branch. They point in the direction of a new branch, which is discovered with a separate run of the continuation algorithm. Bifurcations point out the correlation of different solution branches. An example is that hopping with a very small forward velocity is nearly indistinguishable from hopping on spot with the same CoM height. These two solutions lie on two different branches, but are both close to the bifurcation point, where the hopping on spot motion develops into a forward hopping motion.

Chapter 3

Non-Conservative SLIP Model

The non-conservative SLIP model is developed as an intermediate step towards our goal of transferring the results of the natural gait analysis of the extended SLIP model to a physically realizable model of a legged system. The following key features let our model overcome physically impossible characteristics of the extended SLIP model:

Contact Dynamics The system takes contact dynamics into account, which result from a finite leg mass. This is implemented with a non-zero foot point mass.

Damping The system accounts for friction, which is present in all physically realizable mechanical systems. This is modeled with viscous damping.

Thrust Contact dynamics and friction both result in energy loss of the system. This is compensated for by a mechanism called 'Thrust', which adds energy to the system by increasing the rest length of the spring acting along the leg axis.

The exact implications and realizations of these features will be elaborated on in Sections 3.2.

3.1 Dynamic Model

The model consists of a body mass m_b with fixed rotation and a comparatively small foot point mass m_f. The world position of the body is given by (x, y). The position of the foot with respect to the body is given in polar coordinates, with radius l and angle α. These properties will be denoted as leg length (or leg axis) and leg angle. The latter is zero if the foot CoM is directly below the body CoM.

The absolute positions of the body and foot mass with respect to a ground-fixed coordinate system are given in (3.1). The state of the system can be described by the configuration variables $q = \begin{pmatrix} x & y & \alpha & l \end{pmatrix}^T$ and corresponding velocities $\dot{q} = \begin{pmatrix} \dot{x} & \dot{y} & \dot{\alpha} & \dot{l} \end{pmatrix}^T$.

$$\begin{aligned} r_b &= \begin{pmatrix} x \\ y \end{pmatrix} \\ r_f &= \begin{pmatrix} x + \sin(\alpha) \cdot l \\ y - \cos(\alpha) \cdot l \end{pmatrix} \end{aligned} \tag{3.1}$$

The leg axis is modeled as a massless radial spring with resting length l_o, stiffness k_l and damping b_l. The system features a massless polar spring around the body CoM with resting angle α_0, stiffness k_α and damping b_α.

The model is visualized in Figure 3.1, which also lists dimensionless example parameters used in our analysis. The parameters are normalized with respect to the total body mass m_{tot}, leg length l_o, and gravity constant g (see Hof [1996]). The advantage is that dimensionless parameters generalize the solutions and enable easy and fast comparison and transfer of results to other models.

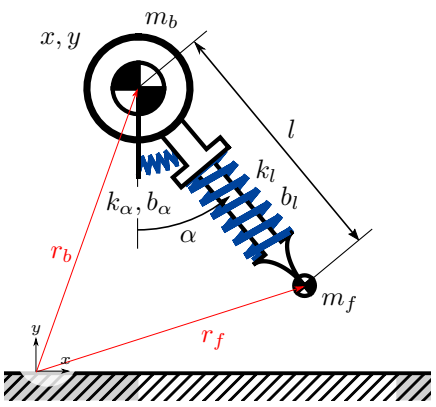

Parameter	Value	Unit
m_{tot}	1	**kg**
l_o	1	**m**
α_o	0	**rad**
g	1	$\mathbf{m/s^2}$
m_b	0.9	m_{tot}
m_f	0.1	m_{tot}
k_l	10	$m_{tot} g / l_o$
k_α	1	$m_{tot} l_o g$
b_l	1	$m_{tot}\sqrt{g/l_o}$
b_α	0.1	$m_{tot} l_o \sqrt{g l_o}$

Figure 3.1: Non-conservative SLIP model with example parameters

3.2 Hybrid Dynamics

The non-conservative SLIP model exhibits both continuous and discrete dynamic behavior and therefore is a hybrid dynamic system.

3.2.1 Continuous Dynamics

Equation (3.2) expresses the continuous dynamics of the hybrid system.

$$M(q)\ddot{q} + b(q,\dot{q}) = -\frac{\partial U_e(q)^T}{\partial q} - d(\dot{q}) + \tau_{ext} \tag{3.2}$$

$$b(q,\dot{q}) = C(q,\dot{q})\dot{q} + \frac{\partial U_g(q)^T}{\partial q} \tag{3.3}$$

$M(q)$ is the positive-definite inertia matrix. The bias force b (3.3) contains the Coriolis and centrifugal forces $C(q,\dot{q})\dot{q}$ and the forces due to the gravitational potential U_g. U_e is the elastic potential energy, and $D\dot{q}$ accounts for dissipative effects of linear viscous damping and friction. τ_{ext} contains external forces between the environment and the model.

The inertia matrix (3.4), the bias forces (3.5), the elastic potential (3.6), and the dissipative term (3.7) are stated explicitly for this one-leg model.

$$M(q) = \begin{pmatrix} m_b + m_f & 0 & \cos(\alpha)\, l m_f & \sin(\alpha)\, m_f \\ 0 & m_b + m_f & \sin(\alpha)\, l m_f & -\cos(\alpha)\, m_f \\ \cos(\alpha)\, l m_f & \sin(\alpha)\, l m_f & l^2 m_f & 0 \\ \sin(\alpha)\, m_f & -\cos(\alpha)\, m_f & 0 & m_f \end{pmatrix} \tag{3.4}$$

$$b(q,\dot{q}) = \begin{pmatrix} \dot{\alpha} m_f \left(\sin(\alpha)\, l\dot{\alpha} - 2\cos(\alpha)\, \dot{l}\right) \\ -\cos(\alpha)\, m_f \dot{\alpha}^2 l - 2\sin(\alpha)\, m_f \dot{\alpha}\dot{l} - g\,(m_b + m_f) \\ -l m_f \left(g\sin(\alpha) + 2\dot{\alpha}\dot{l}\right) \\ m_f \left(\dot{\alpha}^2 l + g\cos(\alpha)\right) \end{pmatrix} \tag{3.5}$$

$$U_e(q) = \frac{1}{2} k_\alpha \left(\alpha - \theta_1\right)^2 + \frac{1}{2} k_l \left(l - \theta_2\right)^2 \tag{3.6}$$

$$d(\dot{q}) = \begin{pmatrix} 0 \\ 0 \\ b_\alpha \dot{\alpha} \\ b_l \dot{l} \end{pmatrix} \tag{3.7}$$

The external forces (3.8) are only non-zero, when the system is in contact with the ground. They are computed using the contact Jacobian J (3.9) and the forces λ resulting from contact.

$$\tau_{ext} = J^T \lambda \tag{3.8}$$

$$J = \begin{pmatrix} 1 & 0 & \cos(\alpha)\, l & \sin(\alpha) \\ 0 & 1 & \sin(\alpha)\, l & -\cos(\alpha) \end{pmatrix} \tag{3.9}$$

The contact forces λ are computed by taking the contact constraints that hold the foot in place into account (3.10).

$$\lambda = -\left(JM^{-1}J^T\right)^{-1}\left(\dot{J}\dot{q} - JM^{-1}\left(b + \frac{\partial U_e^T}{\partial q} + d(\dot{q})\right)\right) \tag{3.10}$$

3.2.2 Discrete Dynamics

The dynamic model undergoes a discrete change at three events during one stride, depicted in Figure 3.2. The ground contact is established at touchdown, the control is activated at thrust, and the ground contact is lost at liftoff. For completeness, the apex event is also introduced here.

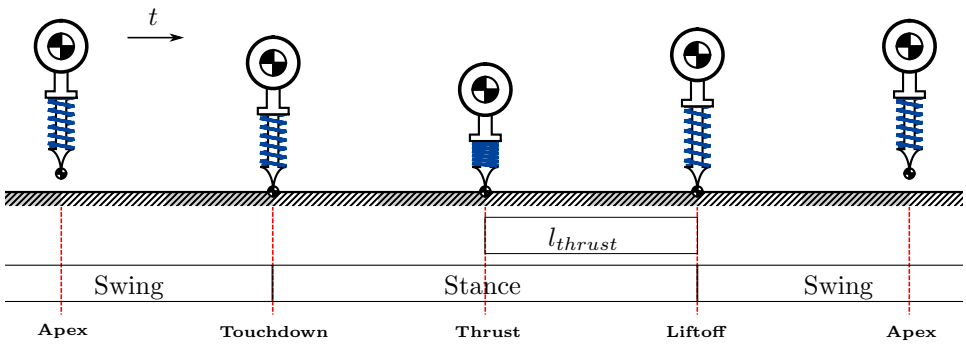

Figure 3.2: One stride of the one-leg hopper

Apex

A stride starts in apex when the body is on its highest position. This corresponds to $\dot{y} = 0$. The system is in swing phase, has no contact to the ground and thrust is not active. Gravity causes the system to fall towards the ground.

Touchdown

The touchdown occurs when the foot hits the ground and its vertical position is zero ($y_{foot} = 0$). The system is now in contact with the ground. The velocity of the foot is reset to zero by changing the impulse of the foot (3.11). The velocities before and after the collision are denoted by $\dot{q}^-$ and $\dot{q}^+$, respectively. This velocity reset causes the kinetic energy of the foot to become zero, which reduces the total energy of the system. After touchdown, the system is in stance phase and the leg spring compresses due to the body mass.

$$\dot{q}^+ = \left(I - M^{-1}J^T\left(JM^{-1}J^T\right)^{-1}J\right)\dot{q}^- \tag{3.11}$$

Thrust

When the leg is the shortest, the leg spring is maximally compressed. The change in spring length ($\dot{l} = 0$) at this time instance is zero and the system switches to thrust phase. The control action 'thrust' is activated and adds energy to the system, amplifying the upwards movement of the body. Adding energy to the system is necessary to compensate the energy loss through 1) the velocity reset of the foot at touchdown and 2) the constantly dissipated energy by damping. Periodic motions of the system can only be found, if the energies of the system at begin and end of one stride are equal.

When the system reaches the thrust phase the resting leg length l_o is artificially increased by l_{thrust}. This increases the deflection of the spring, which correlates to an instantaneous increase $\Delta U_{e,l}$ of the energy stored in the compressed spring (3.12).

$$\Delta U_{e,l} = U_{e,l}^+ - U_{e,l}^- = \frac{1}{2}k_l[(l_o + l_{thrust} - l)^2 - (l_o - l)^2] \tag{3.12}$$

Liftoff

The foot leaves the ground when the contact forces in vertical direction between the foot and the ground are zero ($\lambda_y = 0$). The system transitions into the swing phase. The contact to the ground is lost and thrust is deactivated. In difference to the (extended) SLIP model, the leg length is not held constant during the swing phase. It is purely defined by the dynamics and no active foot lift is incorporated.

Apex is detected when the body reaches its highest position so its vertical velocity $\dot{y}$ vanishes. This marks the completion of one stride.

3.2.3 Energy Fluctuation

There are three reasons why our model is non-conservative. First, the springs are subject to damping to prevent infinite oscillations. This causes the system to dissipate energy. Secondly, the kinetic energy of the foot mass is lost, when the foot hits the ground and its velocity is set to zero. Thirdly, the energy of the system is increased through thrust. It enables us to feed the lost energy back into the system, which is necessary to be able to display periodic solutions.

In Figure 3.3 the changes in total system energy throughout one stride can be seen. Notice the discontinuity in kinetic energy at touchdown, as well as the discontinuity in elastic energy when the thrust is brought into

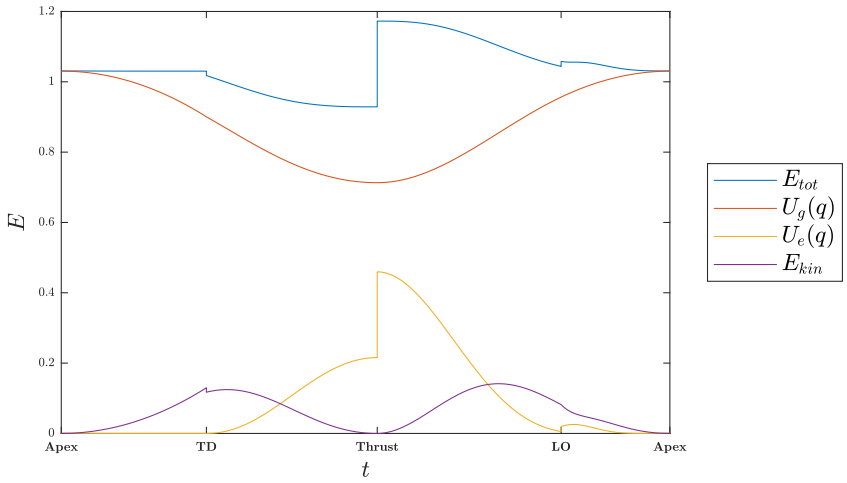

Figure 3.3: System energy during one stride

the system. The effects of damping can be observed when looking at the decreasing total system energy in between the different events.

3.3 Search for Periodic Motions

The integration, respectively simulation of the system was solved in two different, but interchangeable ways.

Event-based integration monitors specific event conditions to detect the appropriate time to stop the simulation. An example of this is monitoring the foot position in the swing phase to detect contact with the ground. This leads to a stop of the solution of the swing dynamics. The ground contact is established and the simulation is now solved taking contact forces (3.10) into account.

Timing-based integration simulates the system until a predefined time. An example for this is simulating the stance dynamics of the system after touchdown for a predefined amount of time, that estimates the next event time. The integration is then stopped, the thrust is activated, and the simulation starts again. After simulating one stride, the solver checks if the event condition at the chosen time was actually fulfilled, and must change the timing variable in order to solve the dynamic system.

For simulation of our hybrid dynamic system, MATLABs `ode45` was used. It solves nonstiff differential equations based on an explicit Runge-Kutta algorithm.

3.3.1 Periodic Motion

Periodic motions are found by using `fsolve`, MATLABs solver for systems of nonlinear equations. It takes an initial guess X^o (3.13) and modifies each component to solve the problem $res(X^o) = 0$.

$$X^o = \begin{pmatrix} x_0 & \dot{x_0} & y_0 & \dot{y_0} & \alpha_0 & \dot{\alpha_0} & l_0 & \dot{l_0} & l_{thrust,0} \end{pmatrix} \tag{3.13}$$

The Poincaré map $P(X^*)$ of the periodic system states X^* (3.14) is built (see Section 2.4). It maps the initial system states X_i of one stride to their respective values X_{i+1} after the stride.

$$X^* = \begin{pmatrix} \dot{x} & y & \dot{y} & \alpha & \dot{\alpha} & l & \dot{l} \end{pmatrix} \tag{3.14}$$

Periodicity is enforced by using the zero function (2.1) as the residuum (3.15).

$$res(X) = P(X) - X \tag{3.15}$$

The Apex is chosen as the Poincaré section, so additionally, the periodic system states need to comply with the apex condition $\dot{y} = 0$.

3.3.2 Event Detection

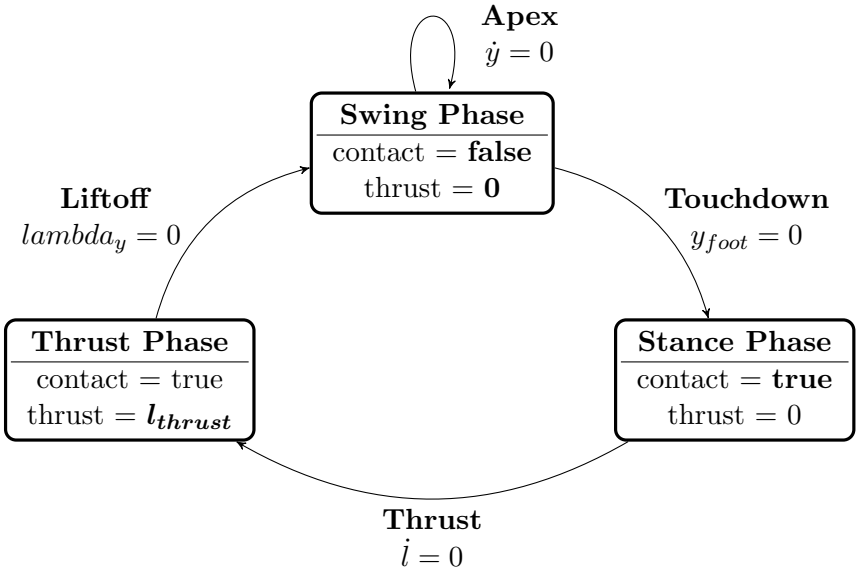

Figure 3.4: State machine for one stride

Figure 3.4 shows the different states of the system during one stride. The event conditions are annotated to the state transitions. The event function of `ode45` monitors the zero crossings of these conditions to detect if an event

is happening. The condition that is monitored changes depending on the system state.

A stride starts in swing phase at apex, which means that the foot is not in contact, the thrust is not active, and the apex condition $\dot{y} = 0$ holds. `ode45` integrates the system step by step while monitoring the touchdown condition. If $y_{foot} = 0$, the integration stops, the system transitions into the stance phase, and the foot now has ground contact. Additionally, the velocity of the foot is reset to zero to model the impact. The simulation starts again, monitoring the thrust condition $\dot{l} = 0$. When fulfilled, the integration stops and thrust is activated. The thrust phase is simulated while monitoring the liftoff condition. When the ground contact forces of the foot vanish, the system transitions into the swing phase and contact and thrust are both reset to zero. The swing phase is simulated until apex is reached and vertical velocity $\dot{y}$ of the body becomes zero.

3.3.3 Timing Variables

The system can also be simulated utilizing timing variables instead of the event detection. An additional timing variable is added to the system for every event.

The simulation starts at time $t = 0$ and simulates the system with deactivated thrust and no ground contact until t_{TD}. This is the initial guess for the time instance when the foot hits the ground. The touchdown condition $y_{foot} = 0$ might not be fulfilled at this time instance. This is taken care of with a timing residuum explained later on. The contact is established and the simulation is continued including contact forces (3.10). The system is then simulated from t_{TD} until t_{THR}, and thrust is activated. The simulation continues until t_{LO}, the ground contact of the foot is broken and thrust is deactivated. From t_{LO} until t_{APEX} the system is simulated using swing phase dynamics.

Timing variables are subject to changes by the solver, similar to the initial system states. To assure that the event conditions are fulfilled at the respective timings, we add a residuum for every event (3.16).

$$\begin{aligned} res_{\mathrm{TD}} &= y_{foot} \Big|_{t_{\mathrm{TD}}} \\ res_{\mathrm{THR}} &= \dot{l} \Big|_{t_{\mathrm{THR}}} \\ res_{\mathrm{LO}} &= F_{contact} \Big|_{t_{\mathrm{LO}}} \\ res_{\mathrm{APEX}} &= \dot{y} \Big|_{t_{\mathrm{APEX}}} \end{aligned} \tag{3.16}$$

3.3.4 Comparison of Event Detection and Timing Variables

Both methods can be used to find periodic gaits, but they have significant differences.

Simulation without the Solver

Event detection enables physically accurate simulations of a stride with any valid initial state, even non-periodic guesses. A valid initial state in apex fulfills the apex condition and the foot of the model is above the ground. Timing-based simulation has the drawback that exact timing variables cannot be known beforehand. Using incorrect timings can result in a foot position above or below the ground when the stance phase is initiated. Therefore timing variables can only be used in combination with the algebraic solver and an appropriate residuum.

Invalid Initial States

The solver might take an invalid initial guess of the system states. For example, the foot position can be below the ground in apex. The event detection will fail to observe the touchdown event and cannot produce a residuum. But without the residuum, the solver cannot improve the guess of the periodic initial states. Using timing variables results in the simulation of a full stride and the display of a proper residuum.

Event Order

Timing variables let the solver choose the order of events. This allows deciding which events need to happen, without restricting solutions to an event pattern. When using event detection, we predefine the order of events as indicated in Figure 3.4. This can lead to undetectable solutions with different event patterns.

Interchangeability

Both methods produce valid solutions, but can not be used abundantly interchangeable. When reading timing variables from a periodic event-based simulation, the timings based simulation also produces a periodic solution, and the event conditions are fulfilled at the timings. Therefore, periodic solutions found by event detection can be transferred without limitations to a simulation using timing variables.

A periodic solution produced with a simulation using timing variables can produce a non-periodic stride when used together with event detection. This will be explained with the example of an oscillating leg in Figure 3.5. The foot swings through the ground with a small Δy. The event detection

will detect the first ground contact e_i^* as the touchdown. The timing-based simulation will report any of the multiple events (i.e. e_{i+2}) where the event condition $y_{foot} = 0$ is fulfilled as touchdown.

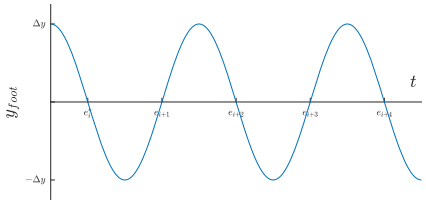

Figure 3.5: Foot mass oscillating around $y = 0$ with events e that fulfill the touchdown condition

3.3.5 Multi-Legged Systems

The `ode45` event function originally intends to monitor all event conditions at once and to detect every single event at the same time. This might work for the one-leg hopper, as every event will only happen once during one stride. For multi-legged systems this usage is problematic.

Consider a bipedal gait shown in Figure 3.6. As mentioned before, the leg length during swing phase is only defined by the swing dynamics of the model. Therefore the swing leg cannot be shortened to not touch the ground during some gaits. The swing of the foot through the ground must not be detected as a touchdown or contact with the ground.

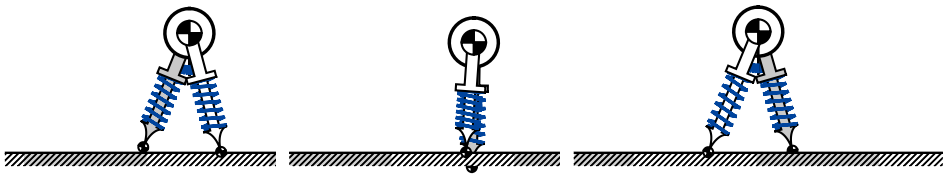

Figure 3.6: Running biped with foot moving through ground

The event detector needs to ignore such events so that the biped does not stumble. In contrary, the timing-based simulation solves this problem inherently. The only precondition is an arbitrarily good initial guess of the event timings.

From the extensive analysis of the extended biped SLIP model by Gan et al. [2018b] we know the chronological order of the events happening in

the different bipedal gaits. This allows us to predefine the order of events without missing possible gaits.

This translates to systems with a different number of legs. The natural gait analysis of a conservative SLIP model provides guidance for the event-based search of gaits of non-conservative SLIP models.

3.4 Bipedal Model

This section explains how the dynamic model of a one-leg hopper can be extended to a bipedal system. The hybrid dynamics are similar, as well as the search for periodic orbits.

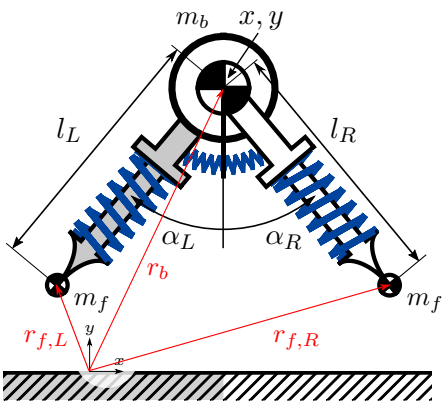

Parameter	Value	Unit
m_{tot}	1.2	**kg**
l_o	1	**m**
α_o	0	**rad**
g	1	$\mathbf{m/s^2}$
m_b	0.83	m_{tot}
m_f	0.08	m_{tot}
k_l	16.67	$m_{tot}g/l_o$
k_α	0.42	$m_{tot}l_o g$
b_l	1.67	$m_{tot}\sqrt{g/l_o}$
b_α	0.04	$m_{tot}l_o\sqrt{gl_o}$

Figure 3.7: Non-conservative bipedal model with example parameters

The bipedal model was developed by adding a second leg - identical to the first one - to the one leg model introduced in Section 3.1. The system state can be fully described by (3.17), giving the positions and velocities of the configuration variables.

$$\begin{aligned} q &= \begin{pmatrix} x & y & \alpha_R & l_R & \alpha_L & l_L \end{pmatrix}^T \\ \dot{q} &= \begin{pmatrix} \dot{x} & \dot{y} & \dot{\alpha}_R & \dot{l}_R & \dot{\alpha}_L & \dot{l}_L \end{pmatrix}^T \end{aligned} \tag{3.17}$$

The absolute positions of the body, right foot (R) and left foot (L) mass

with respect to a ground-fixed coordinate system are given in (3.18).

$$
\begin{aligned}
r_b &= \begin{pmatrix} x \\ y \end{pmatrix} \\
r_{f,R} &= \begin{pmatrix} x + \sin(\alpha_R) \cdot l_R \\ y - \cos(\alpha_R) \cdot l_R \end{pmatrix} \\
r_{f,L} &= \begin{pmatrix} x + \sin(\alpha_L) \cdot l_L \\ y - \cos(\alpha_L) \cdot l_L \end{pmatrix}
\end{aligned} \tag{3.18}
$$

The biped model is visualized in Figure 3.7. We chose similar parameters as Gan et al. [2018b] ($m_b = 1kg$, $k_l = 20\frac{m_b g}{l_o}$, $\omega_\alpha = \sqrt{5}\sqrt{g/l_o}$). The body has a mass of $m_b = 1$kg, and each of the feet have a mass of $m_f = 0.1$kg. The leg stiffness is chosen as $k_l = 20\frac{m_b g}{l_o}$. The swing stiffness is computed from the relationship $\omega_\alpha^2 = \frac{k_\alpha}{m_f l_o}$. It resolves to $k_\alpha = 0.5$. These parameters were normalized with $m_{tot} = m_b + 2 \cdot m_f = 1.2$kg to get the dimensionless parameters given in Figure 3.7.

3.5 Gaits

This section reports on the gaits found for our various non-conservative models. First, we introduce our method to transfer the gait solutions of conservative SLIP models to our non-conservative models. After that, we describe the gaits of our models and compare them to gaits found in conservative SLIP models.

3.5.1 Method

This section explains how we implemented the search for natural gaits. It comments on why the methodology that was proposed by Gan et al. [2018b] does not work with non-conservative systems. We explain our method for finding natural gaits of tha actice system and explain how the analysis of conservative systems is crucial for this.

Bifurcation Analysis

The Monodromy matrix J (see also Section 2.4.3) was built using event-based simulation. It evaluates the influence of small changes to a periodic solution of the system on the system states after one stride. The evaluation of the eigenvalues and eigenvectors of M points out the direction of nearby periodic solutions.

A periodic gait of the non-conservative system is not purely defined by the periodic system states, but also by the thrust parameter l_{thrust}. As

this parameter is discrete, it is not affected by the changes in the periodic parameters.

This was compensated for by investigating the continuous total energy of the system (3.19) at the Poincaré section in apex and adding it to the periodic system states.

$$\begin{aligned} T(\dot{q}) &= E_{kin} = \frac{1}{2}\dot{q}^T M \dot{q} \\ U(q) &= U_e + U_g \\ &= \frac{1}{2}(k_\alpha(\alpha - \alpha_o)^2 + k_l(l - l_o)^2) + m_b g y + m_f g(y - \cos\alpha l) \\ E_{tot} &= T(\dot{q}) + U(q) \end{aligned} \tag{3.19}$$

The Monodromy matrix did not have any eigenvalues with the value +1 anymore. This is a requirement for a correctly built Monodromy matrix of a periodic solution. As a consequence, no eigenvector was tangential to the solution branch and bifurcation points could not be found.

It follows that adding the total system energy to the periodic system states does not yield a valid Monodromy matrix. The discrete system state l_{thrust} renders the application of Floquet analysis to this system impossible.

Building on Passive Gaits

We analyzed an extended SLIP one leg model and find its natural gaits using the bifurcation analysis. These passive gaits, defined by their initial states, are used as a basis for our search of gaits of the non-conservative SLIP model. The differences between the various gaits allow for a targeted search for specific gaits. The process persists of two separated simulation runs, described in the following:

First Solver Run The parameters l, $\dot{l}$, and l_{thrust} need to be adjusted to a given passive gait solution. The parameter states $X^* = \begin{pmatrix} x & \dot{x} & y & \dot{y} & \alpha & \dot{\alpha} \end{pmatrix}$ on the Poincaré section of the passive gait are prescribed to their respective active counterparts. The missing parameters l, $\dot{l}$, and l_{thrust} of the active system are chosen arbitrarily. The solver is tasked with finding a periodic motion, while not altering the parameters taken from the passive solution. This step is necessary because the problem is badly scaled. Unfit parameters l, $\dot{l}$, and l_{thrust} won't result in finding a periodic gait of the non-conservative system.

Second Solver Run After l, $\dot{l}$, and l_{thrust} are adjusted, the search for a periodic orbit is started again. All state variables are set free to be manipulated by the solver. While the first step can yield approximately nearly periodic solutions, the second step is necessary to accurately solve the problem.

Solution branches are discovered using the continuation method described in Subsection 2.4.2. Close-by solutions are predicted assuming a constant development of the solution branch (2.5).

3.5.2 One-Leg Hopper

An extended SLIP One-Leg Hopper (see Section 2.2) was developed. It was parametrized to have the same leg angle eigenfrequency $\omega_{\alpha,sw}$ in swing, and the same leg length eigenfrequency $\omega_{l,st}$ in stance as the non-conservative one leg hopper (see Table 3.1). The natural gaits found for this passive model were used to discover periodic orbits of the non-conservative SLIP model.

Phase	ω_α	ω_l
Swing	3.16	10
Stance	1.05	3.33

Table 3.1: Eigenfrequencies of the non-conservative SLIP one-leg hopper $[\omega] = \sqrt{g/l_o}$

Conservative SLIP Model

In the following, we report on the gaits found for the extended SLIP one-leg hopper. Figure 3.8 shows a projection of the initial states to the three-dimensional parameter space of $\dot{x}$, y, and $\dot{\alpha}$.

Hopping in Place (HP) The characterization of HP is that all values of the state vector in apex are zero, except for y. This gait can be found in the range of $y = [l_o, \frac{k_l}{2mg}]$. The lower end of the value range is defined by the resting leg length. The upper end is defined by a fully compressed leg spring during the stance phase. Starting from $y = 1$ the eigenvectors of the Monodromy matrix corresponding to the eigenvalue $+1$ strictly point in positive y direction. The solutions found along this branch have increasingly longer flight phases and higher velocity during touchdown. In addition, they feature greater spring compression in stance phase.

We find 13 bifurcations along the hopping in place solution branch. The first six are covered below. The additional eigenvectors corresponding to an eigenvalue of $+1$ all feature components in the $\dot{x}$, α, and $\dot{\alpha}$ direction. The solution branches starting at these bifurcation points all correspond to forward (and backward) galloping gaits. The branches extend symmetrically in positive and negative $\dot{x}$ direction. Only the positive velocity range is displayed.

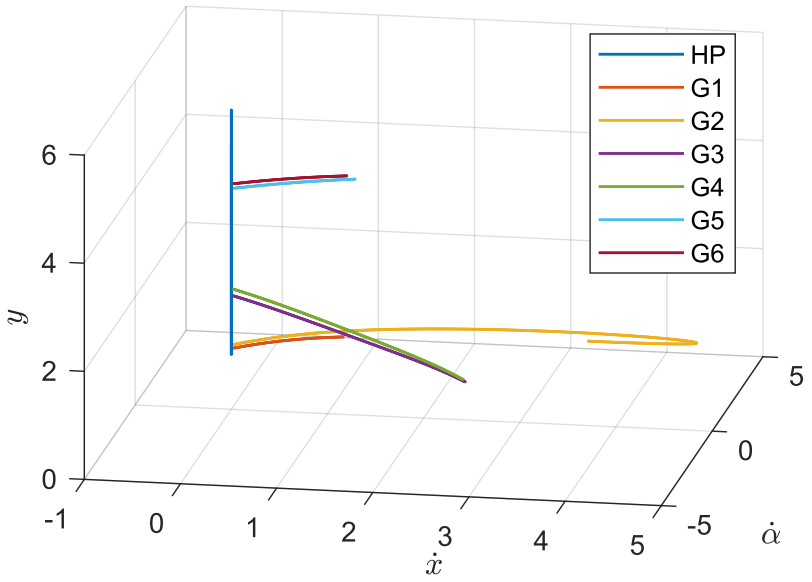

Figure 3.8: Gaits of the conservative one-leg hopper emerging from hopping in place

Galloping Forward (G1 - G6) G1 and G2 are characterized by one swing oscillation of the leg during a stride. In G1 the leg first swings forward under the body and hits the ground during the forward motion. Therefore one can observe a jump and a change of sign in leg angle velocity $\dot{\alpha}$ when the touchdown happens. The leg then swings behind the body, lifts off the ground and begins to swing forward again. In G2 the leg is always vertically beneath the body in apex. It swings forward but starts swinging back again before it touches the ground. This phenomenon known as 'swing leg retraction' (Seyfarth et al. [2003]) is widely found in nature, as it reduces the relative velocity of the foot with respect to the ground. This results in less energy loss through touchdown. While in stance phase the leg moves behind the body, lifts off the ground and swings forward again.

G3 and G4 both incorporate an additional swing oscillation of the leg during flight phase. In apex, the leg swings backward and then forwards again. In G3 the leg hits the ground while swinging forwards, whereas in G4 the leg retracts before touchdown, just like in G2. The leg then moves behind the body while in stance. After liftoff, it swings to the front and back again until apex is reached. In G4 the leg angle α in apex is always zero.

G5 and G6 follow the same pattern as the other gaits. They show three oscillations of the leg in total during one stride. G5 displays the discontinuity in swing leg velocity $\dot{\alpha}$ in touchdown, whereas G6 displays swing leg retraction.

Non-Conservative SLIP Model

In the following, we report on the gaits found for the non-conservative SLIP one-leg hopper. Figure 3.9 projects the initial states of the solutions to the three-dimensional parameter space of $\dot{x}$, y, and $\dot{\alpha}$.

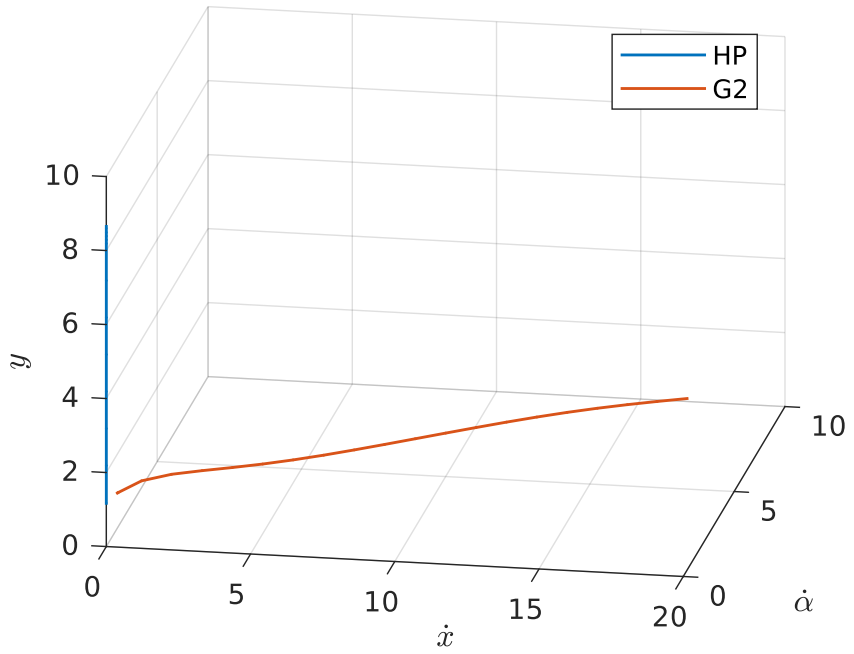

Figure 3.9: Gaits of the non-conservative one-leg hopper emerging from hopping in place

Hopping in Place (HP) We used the method described in Subsection 3.5.1 to find a first solution on the hopping in place solution branch for the non-conservative model. We then used continuation to find a solution in a small distance along the branch.

In apex the system states x, $\dot{x}$, $\dot{y}$, α, $\dot{\alpha}$ are zero. The body height y is steadily increasing along the branch. The leg length l is always approximately l_o and its velocity $\dot{l}$ zero. For very small y the leg is still oscillating when reaching the apex and therefore the values of l and $\dot{l}$ deviate from these values. The parameter l_{thrust} is increasing along with y.

Solutions can be found in the range $y \in [1.07l_o, 8.78l_o]$. The values of thrust are in the range of $l_{trust} \in [0.07l_o, 0.72l_o]$. It can directly be seen, that the non-conservative model can reach higher apex configurations than the passive model. The highest configuration of the extended SLIP model was defined by the maximum energy that can be stored in the system

during highest spring compression in stance phase. In comparison, the non-conservative model can have higher system energy in the apex. It loses the additional energy through damping and the impact at touchdown before the spring is maximally compressed in stance phase.

Galloping Forward (G2) We could find one forward galloping gait of the non-conservative model. It shows the characteristics of the G2 gait of the conservative model. The bifurcation happens at $y = 1.21l_o$ on the HP branch. In apex, the leg is behind the body. This is different from the conservative model, where the leg is directly beneath the body in the apex. The leg then swings forward. Before it touches the ground it swings backward, clearly showing the characteristics of 'swing-leg retraction'. While the foot is on the ground, the body moves over the foot point. The leg starts to swing forward again after liftoff. The system shows only one swing leg oscillation when being in the air. We could find gaits with forward velocities up to $\dot{x} = 18.04\sqrt{gl_o}$ and the maximum thrust used was $l_{thrust} = 4.37l_o$.

Comparison of Extended and Non-Conservative Model Gaits

The non-conservative SLIP model does not display any gait without swing-leg retraction. When the model is forced to place the foot on the ground, while the leg swings forward, the body cannot be vaulted over the foot point. An explanation of this behavior can be found when examining the velocity of the leg angle. The velocity reset of the foot velocity in touchdown does not lead to a change of sign of $\dot{\alpha}$. The forward motion of the system changes to a backward motion within the step and the leg pushes the body towards the ground. A periodic solution cannot be found. Therefore, the non-conservative model does not display any gaits comparable with the gaits G1, G3, and G5 of the extended SLIP model.

The active model also does not display any gait where the leg shows more than one swing oscillation in the air. This results from the damping of the torsional spring. It causes the system to reach its maximum deflection of the torsional spring only once. The gaits G4 and G6 of the passive model thus have no counterpart in the active model.

3.5.3 Biped

The study of Gan et al. [2018b] analyzed a passive extended SLIP model (Section 2.2). Corresponding gaits of the non-conservative bipedal model have been given the same identifier. Bipedal models offer a variety of footfall patterns when hopping in place.

Gaits where the two legs alternately touch the ground have a symmetrical single stance footfall pattern. We defined the order of events of these gaits

as Apex, TD_R, $Thrust_R$, LO_R, Apex, TD_L, $Thrust_L$, LO_L, and Apex. Both legs perform the exact same motion, just half a stride out of phase.

Gaits with fully synchronized legs have an asymmetrical double stance footfall pattern. The touchdown, thrust, and liftoff events of both legs happen at the exact same time.

Symmetrical Single Stance

The gaits with a symmetrical single stance footfall pattern being considered are the running-in-place gait (RP) and a running-forward gait (R2). Figure 3.10 shows a projection of the initial states to the three-dimensional parameter space of $\dot{x}$, y, and $\dot{\alpha}$.

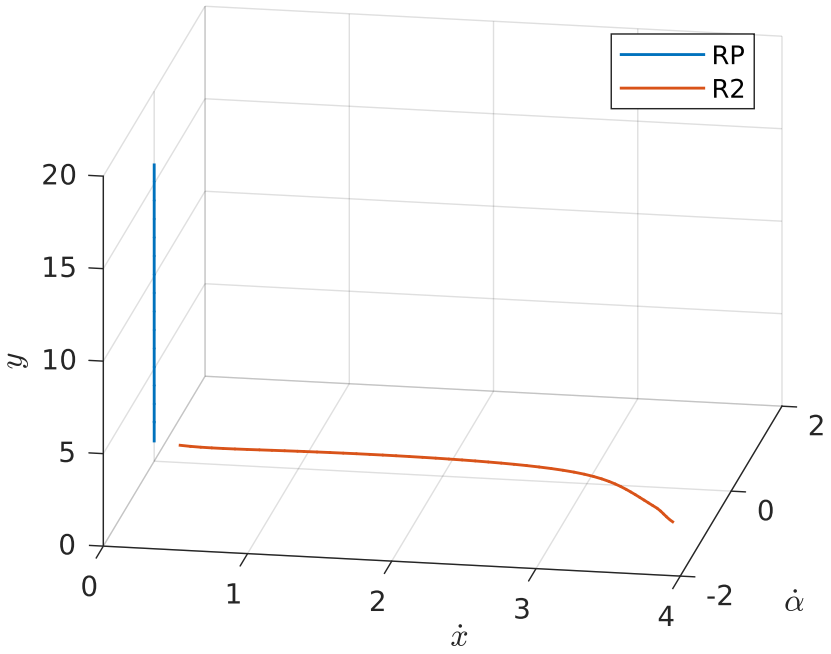

Figure 3.10: Gaits emerging from bipedal symmetrical single stance hopping in place

Running-in-Place (RP) In apex the system states x, $\dot{x}$, $\dot{y}$, α_R, $\dot{\alpha_R}$, α_L, and $\dot{\alpha_L}$ are zero. The body height y is steadily increasing along the branch. The leg lengths l_R and l_L are always approximately l_o and the corresponding velocities zero. The parameter l_{thrust} is steadily increasing with higher y.

Solutions can be found in the range $y \in [1.09l_o, 16.06l_o]$. The thrust required to reach the highest apex position is $l_{thrust} = 0.93l_o$. Again, this model reaches higher body CoM positions than the passive model. The

maximum energy in apex is not directly defined by the maximum energy that can be stored in a fully compressed leg spring.

Running-Forward (R2) Solutions on this branch evolve with increasing forward velocity and incorporate leg swing. The motions found along the R2 branch closely resemble running gaits in nature. The leg angles follow a quasi-sinusoidal trajectory. The legs display swing-leg retraction. The leg moves backward before the foot hits the ground, and the energy loss through touchdown is minimized by matching the velocities of the foot and the ground.

The bifurcation happens at $y = 1.04l_o$ on the RP branch. Solutions have a forward velocity of up to $\dot{x} = 3.64\sqrt{gl_o}$ with thrust reaching $l_{thrust} = 0.48l_o$.

Asymmetrical Gaits

The gaits considered are the hopping-in-place gait (HP) and a galloping gait (G2). The angle α of the right and left leg - as well as leg length l and corresponding velocities - have an equal magnitude for both legs during the whole stride. Figure 3.11 shows a projection of the initial states to the three-dimensional parameter space of $\dot{x}$, y, and $\dot{\alpha}$.

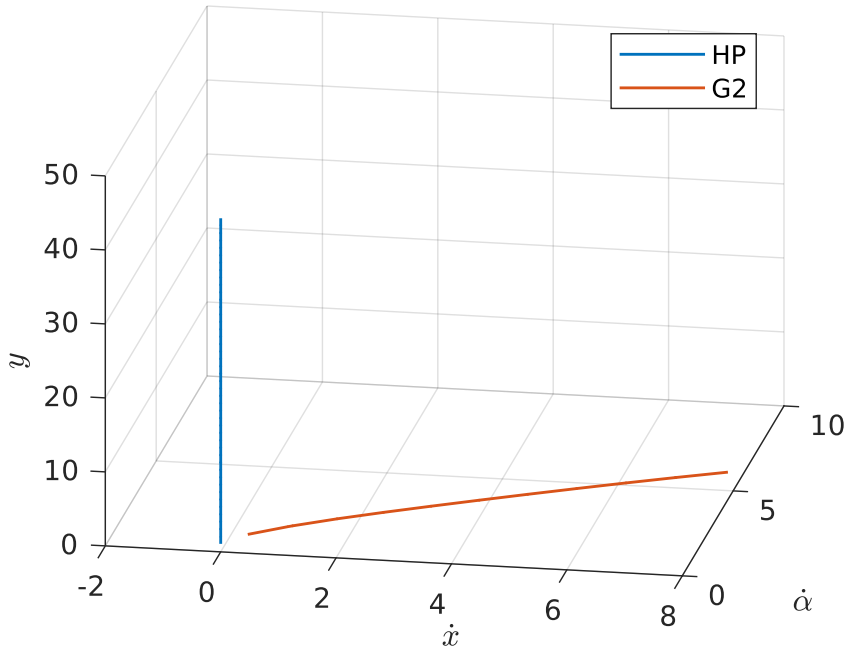

Figure 3.11: Gaits emerging from bipedal asymmetrical double stance hopping in place

Hopping-in-Place (HP) The branch incorporates hopping on spot with a body CoM position in $y \in [1.08l_o; 45.03l_o]$. The thrust parameter ranges in $l_{thrust} \in [0.07l_o; 1.71l_o]$. This gait reaches higher body CoM positions than RP. In stance, the energy stored in the springs is doubled, as both legs are in contact with the ground simultaneously.

Galloping (G2) This gait reaches forward velocities of up to $\dot{x} = 8.64\sqrt{gl_o}$, with a maximum thrust of $l_{thrust} = 1.70l_o$. As all gaits of non-conservative models with forward velocity, the leg is retracted prior to ground contact.

Chapter 4

Pantograph Leg

The goal of this chapter is to design a segmented leg with a dynamic that closely resembles the dynamics of the non-conservative SLIP model. Periodic motions of segmented legs are usually achieved through some sort of control, that changes the intrinsic dynamics of the system. By matching the dynamics of this pantograph leg to those of the non-conservative SLIP model, the control that is necessary to achieve periodic motions can be reduced to purely compensating energy losses. When comparing the pantograph leg with the SLIP model, we are referring to the model described in Chapter 3.

4.1 Dynamic Model

The system consists of a trunk point mass m_t and a thigh, shank, and foot with masses $m_{1..3}$. The lengths, CoM inertias, and CoMs are denoted by $l_{1..3}$, $I_{1..3}$ and $c_{1..3}$, respectively, with the CoM position at half the link length $c_i = \frac{l_i}{2}$. The model is planar and the trunk position is given by (x, y). The thigh is connected to the trunk by a hinge joint with an angle q_1 and the knee is attached to the thigh by a hinge joint with angle q_3. The system features a pulley, which is concentric to the hip and implements a coupling between the the pulley, the hip, and the knee joint $q_3 = \beta(q_2 - q_1)$. The parameter β adds an additional design degree of freedom. The ankle is hinged to the shank via angle q_4. The leg features a pantograph mechanism, which kinematically constrains the foot in parallel with the thigh $q_4 = -q_3$. The contact between foot and ground is modeled as a point. The model is visualized in Figure 4.1.

The minimum set of coordinates is given by $q = \begin{pmatrix} x & y & q_1 & q_2 \end{pmatrix}^T$, which together with the corresponding velocities $\dot{q} = \begin{pmatrix} \dot{x} & \dot{y} & \dot{q}_1 & \dot{q}_2 \end{pmatrix}^T$ defines the state of the system.

The hip joint angle q_1 and pulley angle q_2 are actuated by linear springs with stiffness $k_1 = k_{lin}$ and $k_2 = \alpha k_{lin}$, and are subject to damping $b_1 = b_{lin}$ and $b_2 = \alpha b_{lin}$.

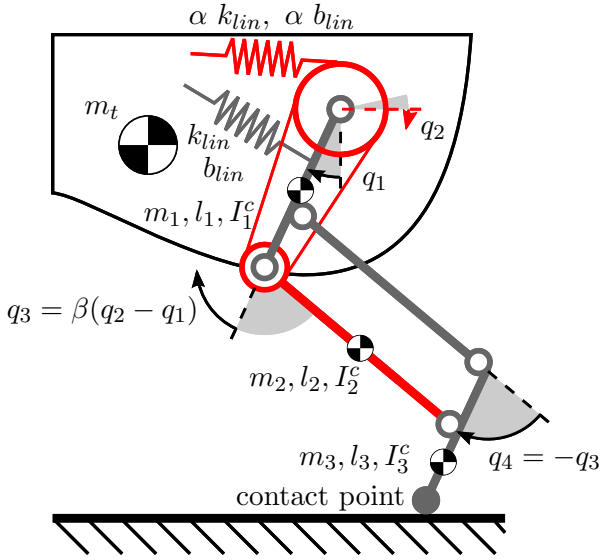

Figure 4.1: Three-segmented pantograph-leg mechanism *(Adapted from Lakatos et al. [2017])*

4.2 Hybrid Dynamics

The hybrid dynamics of the pantograph leg are similar to the ones of the non-conservative SLIP model. Extensive details can be found in Section 3.2.

The continuous dynamics can be expressed by (4.1).

$$M(q)\ddot{q} + b(q,\dot{q}) = -\frac{\partial U_e(q)^T}{\partial q} - d(\dot{q}) + \tau_{ext} \tag{4.1}$$

$$b(q,\dot{q}) = C(q,\dot{q})\dot{q} + \frac{\partial U_g(q)^T}{\partial q} \tag{4.2}$$

$M(q)$ is the positive-definite inertia matrix. The bias force b (4.2) contains the Coriolis and centrifugal forces $C(q,\dot{q})\dot{q}$ and the gravitational potential U_g. U_e is the elastic potential energy, and $d(\dot{q})$ accounts for dissipative effects like viscous damping and friction. τ_{ext} contains external forces between the environment and the model.

The external forces (4.3) are only non-zero when the system is in contact with the ground. They are computed using the contact Jacobian J and the forces λ resulting from contact.

$$\tau_{ext} = J^T\lambda \tag{4.3}$$

The contact forces λ are computed by taking the contact constraints that hold the foot in place into account (4.4).

$$\lambda = -\left(JM^{-1}J^T\right)^{-1}\left(\dot{J}\dot{q} - JM^{-1}\left(b + \frac{\partial U_e^T}{\partial q} + d(\dot{q})\right)\right) \tag{4.4}$$

The system transitions four phases during one stride. The conditions for phase transitions are formulated in task coordinates. The mapping $f(q)$ from joint to task coordinates is given in the next section. The stride starts in apex, when $\dot{y} = 0$. The system has no contact to the ground and thrust is not active. The touchdown occurs when the vertical position of the foot is zero ($y_{foot} = 0$). The system is now in contact with the ground. The velocity of the foot is reset to zero by changing the impulse of the foot (4.5). The velocities before and after the collision are denoted by $\dot{q}^-$ and $\dot{q}^+$, respectively.

$$\dot{q}^+ = \left(I - M^{-1}J^T\left(JM^{-1}J^T\right)^{-1}J\right)\dot{q}^- \tag{4.5}$$

When the leg is spring is fully compressed ($\dot{l} = 0$) thrust is activated. Herein lies a major difference to the application of l_{thrust} in the non-conservative SLIP model. As a reminder, l_{thrust} is used to feed energy into the system and artificially increases the resting length $l_{des} = l_o + l_{thrust}$ of the leg. The pantograph leg is physically constraining l_{des} to its maximal total leg length $l_{des} \leq l_{tot} = l_1 + l_2 + l_3$. When looking at the resulting resting joint angles $q_{1,o}$ and $q_{2,o}$ it becomes evident that by further pretensioning the corresponding springs the energy in the system increases, while the desired leg length shortens and the knee bend direction changes. Therefore the following rule is implemented:

If l_{des} exceeds l_{tot}, the desired resting leg length l_{des} shortens by the $\Delta l = l_{des} - l_{tot}$ by which the total leg length was exceeded and the knee bend direction is reversed.

The liftoff happens, when the contact forces between the foot and the ground are zero ($F_{contact} = 0$). The contact to the ground is lost and thrust is deactivated. The stride is completed with the next apex event.

4.3 Modal Dynamics Matching

The pantograph leg is parametrized to obtain SLIP-like dynamics. The non-conservative SLIP model is used as a template. Its decoupled dynamics are embodied in the design of the pantograph leg.

Investigation of the dynamics in stance (Lakatos et al. [2017]) and in swing (Eßer [2018]) reveals that the design conditions (4.3) must hold, regardless of system state.

$$l_2 = l_1 + l_3 \tag{4.6}$$

$$I_1^c - I_2^c + I_3^c = \frac{(3m_1 + m_2)}{4} l_1^2 + \frac{(2m_1 + m_2)}{2} l_1 l_3 - \frac{(4m_2)}{4} l_3^2 \tag{4.7}$$

$$- \frac{(m_1 + m_2)}{4} l_1 l_3 \tag{4.8}$$

$$\alpha = \frac{\beta}{2 - \beta} \tag{4.9}$$

Additionally to these conditions, all parameters need to have positive values to be physically realistic.

The overall set of design parameters is given by $\zeta = \zeta_1 \cup \zeta_2 \cup \zeta_3$. $\zeta_1 = (m_1, m_2, m_3, l_1, l_2, l_3, I_1^c, I_2^c, I_3^c)$ contains physical parameters of the leg. $\zeta_2 = (m_t, k_{lin}, b_{lin})$ includes the visco-elastic properties and trunk mass. $\zeta_3 = (\alpha, \beta)$ covers the relational parameters which add two design DoFs to the model. As discussed before, the CoMs $c_i = l_i/2$ of the limbs are at half of the limb length.

4.3.1 Task Coordinates

The mapping f of joint space $\boldsymbol{q} = \begin{pmatrix} x & y & q_1 & q_2 \end{pmatrix}^T$ to task space $\boldsymbol{x} = \begin{pmatrix} x & y & \alpha_{leg} & l \end{pmatrix}^T$ of a so-parametrized leg is given in (4.10).

$$x = f(q) = \begin{pmatrix} x \\ y \\ (1 - \frac{\beta}{2})q_1 + \frac{\beta}{2} q_2 \\ (l_1 + l_3)\sqrt{2(1 + cos(\beta(q_2 + q_1)))} \end{pmatrix} \tag{4.10}$$

The mapping of the joint to task velocities is given in (4.11), using the Jacobian J.

$$\dot{x} = J(q)\dot{q} \tag{4.11}$$

Describing the system in task coordinates leads to a simple specification (4.12) of the absolute position of the trunk mass and the toe. These are equivalent to the positions the body and foot mass of the SLIP model (3.1).

$$\begin{aligned} r_{trunk} &= \begin{pmatrix} x \\ y \end{pmatrix} \\ r_{toe} &= \begin{pmatrix} x + \sin(\alpha_{leg}) \cdot l \\ y - cos(\alpha_{leg}) \cdot l \end{pmatrix} \end{aligned} \tag{4.12}$$

The inverse mapping is not unique, as a configuration in task coordinates α_{leg}, l can be reached with either the knee to the right or to the left (see

Figure 4.2). The mapping which results in positive angles q_1 is given in (4.13). The mapping which results in the opposite knee bend direction is given in (4.14).

$$\begin{aligned} q_1 &= \alpha_{leg} - \frac{\pi}{2} + \frac{\arccos\left(\frac{2l_1^2+4l_1l_3+2l_3^2-l^2}{2(l_1+l_3)^2}\right)}{2} \\ q_2 &= \frac{(-2+\beta)\arccos\left(\frac{2l_1^2+4l_1l_3+2l_3^2-l^2}{2(l_1+l_3)^2}\right) + (-\pi+2\alpha_{leg})\,\beta + 2\pi}{2\beta} \end{aligned} \tag{4.13}$$

$$\begin{aligned} q_1 &= \alpha_{leg} + \frac{\pi}{2} - \frac{\arccos\left(\frac{2l_1^2+4l_1l_3+2l_3^2-l^2}{2(l_1+l_3)^2}\right)}{2} \\ q_2 &= \frac{(2-\beta)\arccos\left(\frac{2l_1^2+4l_1l_3+2l_3^2-l^2}{2(l_1+l_3)^2}\right) + (\pi+2\alpha_{leg})\,\beta - 2\pi}{2\beta} \end{aligned} \tag{4.14}$$

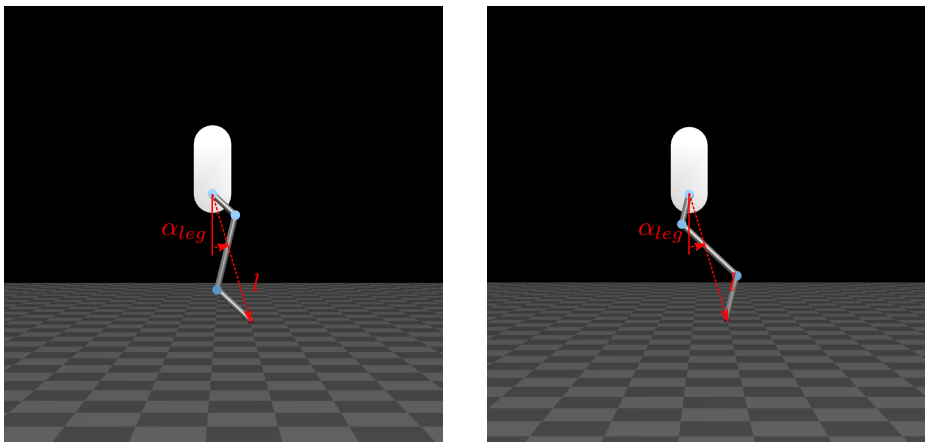

Figure 4.2: Knee-configurations of the pantograph leg

The inverse mapping from task to joint velocities is given by $\dot{q} = J^{-1}\dot{x}$.

A pantograph leg that is parametrized according to these conditions has eigenmodes that separate the high-dimensional coupled dynamics into one-dimensional invariant dynamics. These are equal to the uncoupled dynamics of the SLIP model given by the leg angle α_{leg} and leg axis l. The resting leg length l_o and resting leg angle $\alpha_{leg,o}$ can be modulated as required.

4.4 Search for Optimal Design Parameters

We used a CMA-ES (covariance matrix adaptation evolution strategy) algorithm to numerically optimize the design parameters of the pantograph leg. The population size is set to 100, and the function was evaluated 20 times.

4.4.1 Design Parameters

The pantograph leg is parametrized to be used in the BERT project. The boundary conditions stem from the objective to build a small, dog-like quadrupedal robot.

We started with a fixed set of key parameters, that together with the modal conditions define all design parameters. The initial values for these parameters were taken from Eßer [2018]. The total mass of one leg and a quarter of the trunk is $m_{tot} = 0.6$kg. The ratio of leg mass to body mass is assumed as $m_{leg}/m_{tot} = \eta = 1/6$. The total leg length is set to $l_{leg} = 0.2$m, and the ratio of thigh to foot length is $l_1/l_3 = \gamma = 2/3$. The spring stiffness amounts to $k_{lin} = 2.75$Nm/rad and the relational parameter $\beta = 1$. The aim of the optimization is to match eigenfrequencies, for which we also need to take the resting length of the leg into account. The ratio of resting leg length to total leg length was chosen to be $l_o/l_{tot} = \epsilon = 0.9$.

We gradually freed the different key design parameters, only reaching acceptable eigenfrequencies after all parameters were subject to optimization. Table 4.1 lists the boundaries for the choice of the key design parameters.

Parameter	Range	Unit
m_{tot}	[0.4, 0.6]	kg
η	[0.1, 0.9]	
l_{tot}	[0.2, 0.25]	m
γ	[0.55, 0.93]	
ϵ	[0.5, 0.9]	
β	[0.1, 1.9]	
k_{lin}	[2, 10]	kg/s^2
b/k_{lin}	[0.001, 0.1]	1/s

Table 4.1: Boundary conditions for free design parameters

The optimization algorithm chooses a variable set within these boundaries. The parameters are normalized with total mass m_{tot}, leg length l_{leg}, and gravitational constant $g = 9.81$m/s^2, to continue the optimization with dimensionless parameters. This is important, as our targets for the eigenfrequency matching are also dimensionless.

The additional design parameters were computed as follows: The relative parameter α can be calculated using β (4.15). If the second spring stiffness $k_2 = \alpha k_{lin}$ is outside the stiffness boundaries of k_{lin}, the optimization is aborted.

$$\alpha = \frac{\beta}{2 - \beta} \tag{4.15}$$

The lengths of the thigh, shank, and foot, and the resting leg length are

computed in (4.16).

$$\begin{aligned} l_o &= \epsilon l_{tot} \\ l_{shank} &= l_{tot}/2 \\ l_{thigh} &= \gamma/(1+\gamma) l_{shank} \\ l_{foot} &= l_{shank} - l_{thigh} \end{aligned} \tag{4.16}$$

The dimensionless masses are computed from the modal conditions for the foot mass and the inertia and the total leg mass (4.17). The indices $i \in \{1, 2, 3\}$ denote parameters of the thigh, shank, and foot.

$$\begin{aligned} I_1^c - I_2^c + I_3^c &= \frac{(3m_1 + m_2)}{4} l_1^2 + \frac{(2m_1 + m_2)}{2} l_1 l_3 - \frac{(3m_2 + m_3)}{4} l_3^2 \\ m_3 &= \frac{(m_1 l_1 + m_2(l_1 - l_3))}{l_3} \\ m_{leg} &= m_1 + m_2 + m_3 \end{aligned} \tag{4.17}$$

The total leg mass is computed with $m_{leg} = \zeta m_{tot}$. The inertias were computed with (4.18). The center of mass of a limb is defined to be at half the link length $c_i = l_i/2$. A limb is modeled as a rigid body with two single point masses. The position of those point masses is on the longitudinal axis of the link, with distance $\rho l_i/2$ from the center of mass c_i. The values of ρ were predefined, to maximize the range of γ that leads to positive limb masses. $\rho_1 = 2$ prescribes the point masses to be located outside of the thigh segment between the hip and knee joints. $\rho_2 = 0.125$ describe that the two point masses of the shank are located close to the CoM of the shank. $\rho_3 = 1$ defines that the point masses of the foot are located inside the ankle joint and the toe tip.

$$I_i^c = 1/4 \rho_i^2 m_i l_i^2 \tag{4.18}$$

4.4.2 Eigenfrequency Matching

The eigenfrequencies were computed separately for stance and swing phase.

The inertia matrix M was evaluated in equilibrium leg configuration, where the leg has resting length and angle. M is separated into four 2×2 submatrices (4.19).

$$M(q) = \begin{bmatrix} M_{bb}^{2\times 2} & M_{bj} \\ M_{bj}^T & M_{jj}^{2\times 2} \end{bmatrix} \tag{4.19}$$

The lower right submatrix of the stiffness matrix K contains the joint stiffness of q_1 and q_2 (4.20).

$$K = \begin{bmatrix} 0 & 0 \\ 0 & K_{jj}^{2\times 2} \end{bmatrix} \tag{4.20}$$

The eigenfrequencies in swing phase are approximated by solving the generalized eigenvalue problem (4.21) using the leg inertia matrix in swing $M_{sw} = M_{jj}$ and stiffness matrix $K_{sw} = K_{jj}$ in swing. The eigenfrequencies $\omega_{sw} = \sqrt{\lambda_{sw}}$ are computed from the eigenvalues. The leg angle eigenfrequency $\omega_{sw,\alpha}$ belongs to the eigenvector $v = (1, 1)^T$, and the eigenvector $v = (0, 1)^T$ corresponds to the leg length eigenfrequency $\omega_{sw,l}$.

$$\lambda_{sw} M_{sw} v = K_{sw} v \tag{4.21}$$

The eigenfrequencies in stance phase take the Jacobian of the contact constraint $\Phi_{jb}(q)$ into account (4.22). It describes the foot point in the world. The inertia matrix M_{st} in stance is given in (4.23), and the stiffness matrix K_{st} in (4.24).

$$\Phi_{jb} = \left(\frac{\partial r_{toe}(q)}{\partial [q_1 \; q_2]^T} \right)^{-1} \left(\frac{\partial r_{toe}(q)}{\partial [x \; y]^T} \right) \tag{4.22}$$

$$M_{st} = M_{bb} - M_{bj}\Phi_{jb}(q) - \Phi_{jb}(q)^T M_{bj}^T + \Phi_{jb}(q)^T M_{jj} \Phi_{jb}(q) \tag{4.23}$$

$$K_{st} = \Phi_{jb}(q)^T K_{jj} \Phi_{jb}(q) \tag{4.24}$$

The eigenfrequencies $\omega_{st} = \sqrt{\lambda_{st}}$ are computed from the eigenvalues of (4.25). The leg angle eigenfrequency $\omega_{st,\alpha}$ belongs to the eigenvector $v = (1, 0)^T$, and the eigenvector $v = (0, 1)^T$ corresponds to the leg length eigenfrequency $\omega_{st,l}$.

$$\lambda_{st} M_{st} v = K_{st} v \tag{4.25}$$

In our cost function (4.26), we used the eigenfrequencies of the non-conservative SLIP model (3.1) as the optimization target. We followed an least-squares approach to minimize the difference between the desired and pantograph leg eigenfrequencies. The term for the leg angle eigenfrequency in swing is fully weighted. Our analysis showed that the leg swing in flight phase significantly influences the forward velocities reachable in hopping. The divergence of desired and actual eigenfrequencies in stance phase are weighted with 0.5. The leg length frequency in swing is not considered in the

cost function, as the oscillation behavior of the leg length in swing barely influences the ability of the leg to express periodic gaits.

$$\begin{aligned} \text{cost} = \; & (\omega_{sw,\alpha,des} - \omega_{sw,\alpha})^2 + 0.5 \cdot (\omega_{st,\alpha,des} - \omega_{st,\alpha})^2 \\ & + 0.5 \cdot (\omega_{st,l,des} - \omega_{st,l})^2 + 0.3 \cdot (xi_{sw,\alpha,des} - xi_{sw,\alpha})^2 \end{aligned} \tag{4.26}$$

We also add the least squares term of the damping ratio of the swing leg angle to the cost function, weighted with 0.3, to obtain damping values that do not prohibit the system from swinging. The damping ratio was obtained with the method described by Shaw and Pierre [1993]. The comparability of the pantograph leg with the non-conservative SLIP model would get lost if the damping inside the pantograph leg would be estimated to high.

4.5 Analysis of the Results

The CMA-ES algorithm optimized the dynamics of the pantograph leg to have the eigenfrequencies listed in Table 4.2. The desired values are listed for comparison. The dimensionless desired damping ratio $\xi_{sw,\alpha,des} = 0.1581$ was closely reached with $\xi_{sw,\alpha} = 0.1506$.

Phase	$\omega_{\alpha,des}$	$\omega_{l,des}$
Swing	3.16	10
Stance	1.05	3.33

Phase	ω_{α}	ω_{l}
Swing	3.16	8.77
Stance	1.03	3.37

Table 4.2: Desired and optimized eigenfrequencies of the pantograph leg $[\omega] = \sqrt{g/l_o}$

Table 4.3 lists the optimal design parameters with dimensions, that have been found with the optimization introduced in Section 4.4.

We analyze the influence of the spring stiffness k_{lin} on the optimized eigenfrequencies.

The total body mass and the total leg length are defined as $m_{tot} = 0.4394\text{kg}$ and $l_{tot} = 0.2308\text{m}$ respectively. These are the optimized values given by the numerical optimization in Section 4.4. The spring stiffness is taken from $k_{lin} \in [2\text{N/m}, 10\text{N/m}]$ in steps of 10% of the optimized $k_{lin,opt} = 8.8993\mathbf{N/m}$

The search for optimized design parameters is started with the free parameters η, γ, ϵ, β, b/k_{lin}. Figure 4.3 displays the best optimized eigenfrequencies that could be reached by the CMA-ES algorithm.

The target eigenfrequencies are reached with $k = 100\% \cdot k_{lin,opt}$. When deviating the optimal spring stiffness by 20% in a positive or negative direction, the desired leg angle swing eigenfrequency can still be achieved. The match of the eigenfrequencies in stance is still satisfactory. The influence

Parameter	Value	Unit
m_{tot}	0.4394	**kg**
l_o	0.1985	**m**
α_o	0	**rad**
g	1	$\mathbf{m/s^2}$
m_{trunk}	0.2623	**kg**
m_{thigh}	0.0472	**kg**
m_{shank}	0.1224	**kg**
m_{foot}	0.0075	**kg**
l_{thigh}	0.0500	**m**
l_{shank}	0.1154	**m**
l_{foot}	0.0654	**m**
k	8.8993	**N/m**
b	0.1306	**kg/s**
β	0.4260	
α	0.2706	

Table 4.3: Optimized design parameter set

of the leg length eigenfrequency in the swing phase on the overall motion of the system is negligible. When predefining a spring stiffness of less than 80% of $k_{lin,opt}$ the deviations of all eigenfrequencies from the desired ones become unacceptably large.

We conclude that the large spring stiffness given by the optimizer is necessary to reach the target eigenfrequencies. A small deviation of less than 20% of the optimal spring stiffness leads to acceptable eigenfrequencies but using a spring with significantly smaller stiffness results in smaller eigenfrequencies.

Figure 4.4 shows the optimized mass distribution in dimensionless mass parameters. It can clearly be seen, that a higher spring stiffness results in a heavier leg when compared with the trunk mass. This analysis gives another indication of why the optimal spring stiffness is as high. Smaller stiffnesses lead to a lighter leg, which results in a physically not realizable very small foot mass. The leg mass needs to be at least roughly a third of the total system mass to enable foot segments with a significant mass.

Figure 4.5 shows the influence of the choice of spring stiffness on the length distribution of the thigh, shank, and foot. It can clearly be seen, that the distribution of segment lengths is barely influenced by the deviating stiffnesses. Rather the ratio of the thigh to foot length lies on the end of the parameter range. This boundary cannot be softened, as it would result in negative segment masses.

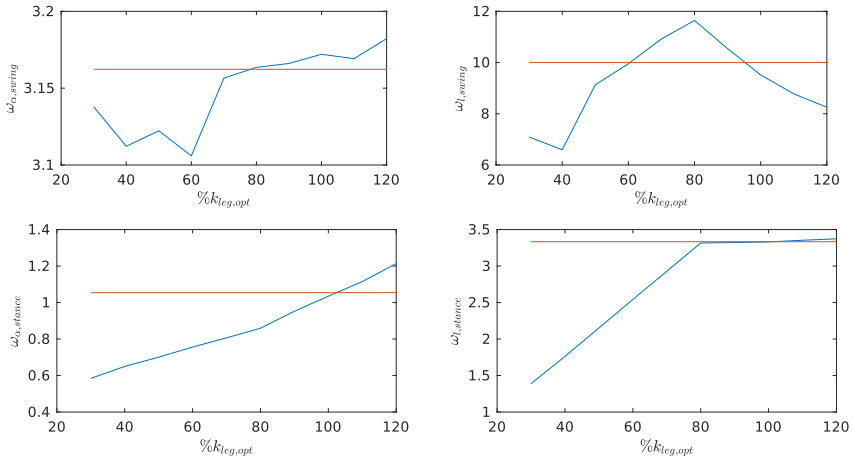

Figure 4.3: Influence of stiffness k on achievable optimal eigenfrequencies $[\omega] = \sqrt{g/l_o}$

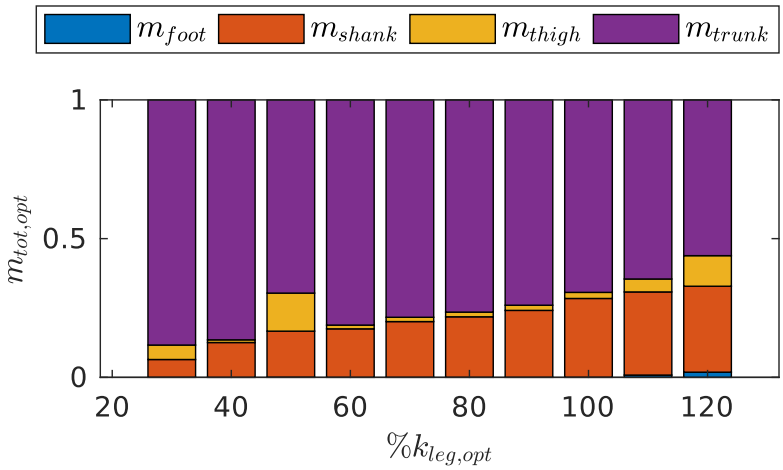

Figure 4.4: Influence of stiffness k on mass distribution

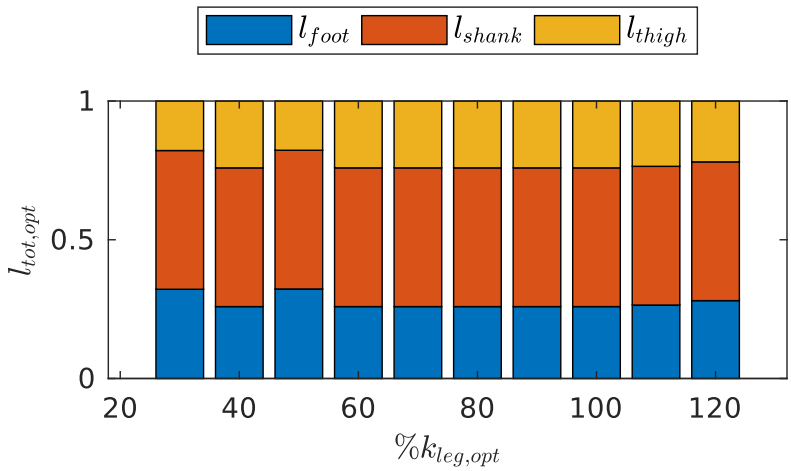

Figure 4.5: Influence of stiffness k on length distribution

4.6 Comparison to Biological Legs

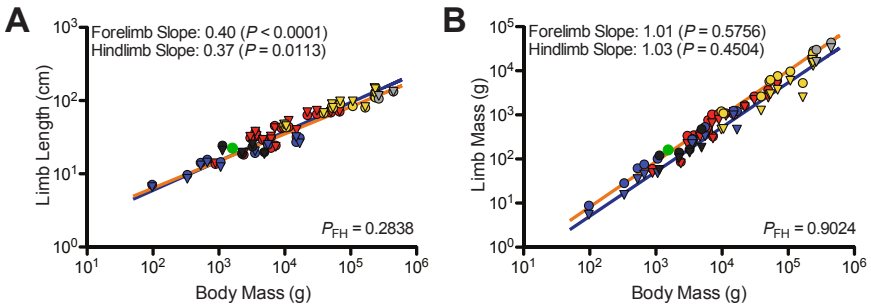

Figure 4.6: Biological limb traits scaled against body mass *(taken from Kilbourne and Hoffman [2013])*

Kilbourne and Hoffman [2013] studied the leg length and inertial properties of 44 species of terrestrial mammals. They showed that leg length scales with positive allometry ($length \propto bodymass^{0.4}$). This can be seen in on the left-hand side of Figure 4.6. The green dot represents the optimized pantograph leg, where the body mass is computed as $bodymass = 4 \cdot m_{tot}$ because we defined m_{trunk} to be a quarter of the total trunk mass. The plot on the right side shows that leg mass scales isometric ($m_{leg} \propto bodymass^{1.0}$).

This analysis shows that the proportions of leg length, leg mass, and total body mass chosen for the pantograph leg are similar to those present in nature.

Chapter 5

Discussion

In the following we interpret our results and compare them to previous studies. Additionally we comment on the limitations of our findings and highlight unexpected results.

The non-conservative SLIP model with minimal control is capable of showing natural gaits. Periodic motions are compared to corresponding gaits of established energy-conservative SLIP models. The dynamics of the developed active model are matched to the dynamics of a pantograph leg.

5.1 Non-Conservative SLIP Model with Minimal Control

A non-conservative SLIP model has been derived. On the contrary to energy-conservative SLIP models introduced in literature until now, it considers contact dynamics and damping. Both lead to energy loss during one stride. It features minimal control, which acts on the translational spring and counteracts the lost energy. This keeps the total system energy in apex constant, which is necessary for the existence of periodic motions.

The control action instantaneously increases the elastic energy stored in the translational leg spring, when this spring is maximally compressed during the stance phase. Therefore, the control acts only on one DoF and acts merely during the second half of the stance phase. This lets us speak of minimal control.

Although only the leg length DoF is subject to control, we could find periodic motions like forward hopping, that clearly incorporate motion in two DoFs of the leg - leg angle and leg length. We can speak of these periodic motions as the natural gaits of the non-conservative SLIP model, as the dynamics of the model are defined by its natural dynamics without control for the majority of a stride - the complete swing phase and the first half of the stance phase.

The minimal control approach lets us find natural gaits in the non-conservative SLIP model.

5.2 Natural Gaits of the Non-Conservative SLIP Models

When comparing the natural gaits of the non-conservative system with their respective ones of the conservative SLIP model, two things are notable:

First, when hopping on spot, the non-conservative model reaches higher body CoM positions. This holds for the one-leg model, as well as for the bipedal model with both footfall patterns - symmetrical single stance and asymmetrical double stance.

The maximum CoM height of the conservative model is defined by the maximum energy that can be stored in the system. When the leg spring fully compresses during the stance phase, the potential and kinetic energy of the system become zero. The maximum total energy of the system is therefore restricted by the energy that can be stored in a fully compressed leg spring.

The non-conservative model is subject to energy fluctuation during one stride. It reaches the lowest total system energy in stance, when the leg spring is maximally compressed and the thrust has not yet been activated. In return, this means that the system energy in apex can be higher, which relates to higher body CoM positions.

Secondly, conservative bipedal models reach higher forward velocities than non-conservative bipedal models. The translational DoF is used to transform kinetic and potential energy in the swing phase into elastic energy in the stance phase. The rotational DoF redirects the leg spring force in stance and adjusts the leg angle during the swing phase for the next ground contact phase.

The minimal control approach only acts on the translational DoF, adding energy to the system. The rotational DoF, on the other hand, is subject to damping. We hypothesize that this impedes the redirection of leg spring force, resulting in a higher body CoM trajectory, shorter stride length, and lower maximum forward velocities. Furthermore, this hypothesis is supported by the fact that the continuation of gaits with a forward motion of the non-conservative model does not end in the singularity of fully compressed leg springs. The maximum forward velocity is rather restricted by the absence of solutions with periodic leg angles and velocities.

Natural gaits of the non-conservative SLIP models reach higher body CoM trajectories, but lower forward velocities, when compared with conservative models.

5.3 Eigenfrequency Matching of the Pantograph Leg

The modal conditions for design parameters lead to reduced, SLIP-like dynamics of the pantograph leg. The solution space for these design parameters results in a large range of possible leg eigenfrequencies. This study proposed a method to match the eigenfrequencies of the pantograph leg to those of an arbitrary SLIP model. Prior to this study, SLIP-like dynamics could be integrated into a pantograph leg, however, the resulting oscillating behavior could not be influenced.

The eigenfrequency matching enables a specification of the characteristics of the SLIP dynamic. It gives a guideline on how to choose design parameters in the large solution space leading to SLIP-like dynamics. Furthermore, matched eigenfrequencies enable the transfer of gait solutions found in simple SLIP models to the pantograph leg and enables a prediction of the maximum jumping heights or maximum forward velocities that can be achieved with the leg.

The eigenfrequencies used in this study as a matching target were chosen arbitrarily. Using a specific mammalian leg as a basis for the pantograph leg enables the indirect measurement of eigenfrequencies from a motion video. Eigenfrequency matching is most likely more accurate than trying to measure and match parameters like the leg length stiffness.

The free design parameters of the pantograph leg were chosen so that the leg compares to the two-segmented legs of the BERT robot. It is notable, that the optimized spring stiffnesses are much higher than expected when compared to the existing ones in the legs of BERT. This might result from the higher leg swing eigenfrequencies.

Chapter 6

Conclusion

This thesis contributes to several aspects of SLIP-like legged locomotion. The concept of SLIP models has been transferred to a physically more realistic model, which is influenced by energy fluctuations during a stride. Additionally, SLIP-like dynamics have been embedded into a physically realizable pantograph leg.

The non-conservative SLIP model has been build to incorporate viscous damping and contact dynamic effects. The resulting energy loss is compensated with a minimal control action. It adds energy into the system by increasing the elastic energy stored in the leg spring. The model exhibits periodic gaits including hopping on spot and forward motions. These motions incorporate a movement of the angular DoF of the leg, although the control is only acting upon the translational DoF of the leg.

The gaits of the active SLIP model can be classified as natural gaits, since the control only adds energy into the system and lasts only half of the stance phase. When comparing the gaits displayed by this active model with gaits reported for conservative SLIP models, two major differences become obvious. While hopping on spot, the non-conservative model reaches higher body CoM positions. But when displaying forward motions, the maximum velocity reached by bipedal models is lower than comparable results of passive bipedal SLIP models. The non-conservative one-leg hopper on the other hand reaches higher velocities than its conservative counterpart.

The pantograph leg has been parametrized to feature SLIP-like dynamics. Additionally, the parameters were chosen with the goal to generate specific leg eigenfrequencies. The motions of this physically realizable segmented leg can be compared to gaits of the SLIP model effortlessly.

Overall, the concept of the SLIP model has been embedded into a physically realistic segmented leg. Findings on gaits exhibited by the SLIP model can be transferred to a pantograph leg, in order to use is for physical robots.

6.1 Future Work

6.1.1 Non-Conservative SLIP Model

Our findings let conclude that choice of how energy is fed back into the system influences the ability of the model to reach certain heights or forward velocities. Therefore, the usage of the control parameter should be evaluated. The following open questions arise:

In our current implementation, the deactivation of the control induces a small amount of energy into the system. Is it possible to control the system less, i.e. a shorter period of time, to disable this side-effect?

The maximum forward velocity reached by the non-conservative SLIP models is significantly lower than the corresponding velocities of conservative models. Is the control of the leg angle necessary, or does this effect arise from the choice of the damping parameter?

The control parameter is equal for all legs of multi-legged SLIP models. Does this limit the ability to express gaits like bipedal skipping, where one leg moves faster than the other and the legs touch (and leave) the ground with different leg angles?

6.1.2 Pantograph Leg

The choice of target eigenfrequencies should be the subject of further research. Various interesting research questions arise:

What are the leg eigenfrequencies of mammals with similar leg length and total body mass?

How do the eigenfrequencies of the leg influence the mass distribution and the spring stiffnesses?

Can the spring stiffnesses be reduced when enabling the leg to shorten during the swing phase?

Do multi-legged models with pantograph legs exhibit natural gaits?

List of Figures

2.1 One stride of a running spring-mass system 4
2.2 Ground reaction forces of the IP model 5
2.3 One stride of a walking bipedal SLIP model 6
2.4 Extended SLIP model 7
2.5 Periodic orbit in the y, $\dot{y}$ plane with marked Poincaré section 7

3.1 Non-conservative SLIP model with example parameters . . . 11
3.2 One stride of the one-leg hopper 13
3.3 System energy during one stride 15
3.4 State machine for one stride 16
3.5 Foot mass oscillating around $y = 0$ 19
3.6 Running biped with foot moving through ground 19
3.7 Non-conservative bipedal model with example parameters . . 20
3.8 Gaits of the conservative one-leg hopper 24
3.9 Gaits of the non-conservative one-leg hopper 25
3.10 Gaits emerging from bipedal symmetrical single stance hopping 27
3.11 Gaits emerging from bipedal asymm. double stance hopping . 28

4.1 Three-segmented pantograph-leg mechanism 31
4.2 Knee-configurations of the pantograph leg 34
4.3 Influence of stiffness k on achievable optimal eigenfrequencies 40
4.4 Influence of stiffness k on mass distribution 40
4.5 Influence of stiffness k on length distribution 41
4.6 Bilogical limb traits scaled against body mass 41

List of Tables

3.1 Eigenfrequencies of the non-conservative SLIP one-leg hopper 23

4.1 Boundary conditions for free design parameters 35
4.2 Desired and optimized eigenfrequencies of the pantograph leg 38
4.3 Optimized design parameter set 39

Bibliography

Reinhard Blickhan. The spring-mass model for running and hopping. *Journal of biomechanics*, 22(11-12):1217–1227, 1989.

Harry Dankowicz and Frank Schilder. *Recipes for continuation*, volume 11. SIAM, 2013.

Julian Eßer. Analysis of a physically implementable pantograph-leg mechanism with slip characteristics. Bachelor's thesis, University of Duisburg-Essen, 2018.

Zhenyu Gan, Ziyuan Jiao, and C David Remy. On the dynamic similarity between bipeds and quadrupeds: a case study on bounding. *IEEE Robotics and Automation Letters*, 2018a.

Zhenyu Gan, Yevgeniy Yesilevskiy, Petr Zaytsev, and C David Remy. All common bipedal gaits emerge from a single passive model. *Journal of The Royal Society Interface*, 15(146):20180455, 2018b.

Hartmut Geyer, Andre Seyfarth, and Reinhard Blickhan. Compliant leg behaviour explains basic dynamics of walking and running. *Proceedings of the Royal Society of London B: Biological Sciences*, 273(1603):2861–2867, 2006.

At L Hof. Scaling gait data to body size. *Gait & posture*, 3(4):222–223, 1996.

Brandon M Kilbourne and Louwrens C Hoffman. Scale effects between body size and limb design in quadrupedal mammals. *PLoS One*, 8(11):e78392, 2013.

Dominic Lakatos, Werner Friedl, and Alin Albu-Schäffer. Eigenmodes of nonlinear dynamics: Definition, existence, and embodiment into legged robots with elastic elements. *IEEE Robotics and Automation Letters*, 2 (2):1062–1069, 2017.

Simon Mochon and Thomas A McMahon. Ballistic walking. *Journal of Biomechanics*, 13(1):49–57, 1980.

André Seyfarth, Hartmut Geyer, and Hugh Herr. Swing-leg retraction: a simple control model for stable running. *Journal of Experimental Biology*, 206(15):2547–2555, 2003.

Steven W Shaw and Christophe Pierre. Normal modes for non-linear vibratory systems. 1993.